NASA-CR-192981

AERODYNAMIC ANALYSIS OF HYPERSONIC WAVERIDER AIRCRAFT

GRANTOR-NASA AMES RESEARCH CENTER

GRANTEE-CAL POLY STATE UNIVERSITY

GRANT NUMBER NAG 2-766

10/01/91 - 09/30/93

Principal Investigator

Dr. Doral R. Sandlin

Student Investigator

David N. Pessin

Cal Poly State University
San Luis Obispo, CA 93407

April 1993

ABSTRACT

AERODYNAMIC ANALYSIS OF HYPERSONIC WAVERIDER AIRCRAFT

by

David Neil Pessin

The purpose of this study is to validate two existing codes used by the Systems Analysis Branch at NASA Ames Research Center, and to modify the codes so they can be used to generate and analyze waverider aircraft, both at on-design and off-design conditions.

To generate waverider configurations and perform the on-design analysis, the appropriately named Waverider code is used. The Waverider code is based on the Taylor-Maccoll equations. Validation is accomplished via a comparison with previously published results. The Waverider code is modified to incorporate a fairing to close off the base area of the waverider configuration. This creates a more realistic waverider.

The Hypersonic Aircraft Vehicle Optimization Code (HAVOC) is used to perform the off-design analysis of waverider configurations generated by the Waverider code. Various approximate analysis methods are used by HAVOC to predict the aerodynamic characteristics, which are validated via a comparison with experimental results from a hypersonic test model.

TABLE OF CONTENTS

	Page
LIST OF FIGURES	iv
NOMENCLATURE	vi
Introduction	1
Background	1
Related Codes	2
Purpose of Study	4
Waverider Concept	5
Idealized Cone-derived Waverider	5
General Cone-derived Waverider	6
Waverider Computer Code	8
Conical Flow	9
The Taylor - Maccoll Equation	11
Fairing Generation	15
Prandtl-Meyer Flow	17
HAVOC Computer Code	22
AEROSA Code	22
Tangent Wedge Theory	24
Newtonian Theory	30
Results & Discussion	33
Introduction to Results	33
Comparison of Three Waveriders with Published Configurations	33
Configuration 1	35
Configuration 2	35

Configuration 3 35
Summary 36
Comparison of HAVOC Code with Experimental Results 43
The All-Body Hypersonic Test Model 43
Mach 2.0 Results 45
Mach 5.37 Results 46
Mach 7.38 Results 46
Mach 10.6 Results 47
Summary 48
Mach 8 Waverider Analysis 54
Effect of Fairing and Engine on Waverider Performance 54
Comparison of Analysis Methods 59
Pitching Moment and Force Coefficient Results 61
Mach 14 Waverider Analysis 66
Comparison of Analysis Methods 68
Pitching Moment and Force Coefficient Results 69
Conclusions 73
References 76
Appendix: Original Computer Code Listings 78
Fairing Generation and Modification Routines for Waverider Code ... 78
Section of Subroutine WAVRDR 78
Subroutine PARABOLA 81
Subroutine FAIRANAL 84
Elevator Generation Routines for HAVOC 90
Section of Subroutine AEROANAL 90
Subroutine ELEVATOR 91

LIST OF FIGURES

		Page
Figure 2.1.	Idealized Conical Waverider	6
Figure 2.2.	General Conical Waverider	7
Figure 3.1.	Conical Flow field	10
Figure 3.2.	Cylindrical Coordinate System	10
Figure 3.3.	Conical Coordinate System	11
Figure 3.4.	Waverider with Fairing(View of Lower Surface)	17
Figure 3.5.	Parabolic Curve Describing Fairing	17
Figure 4.1.	Supersonic Flow Past a Wedge	29
Figure 4.2.	Flow Crossing Shock	29
Figure 4.3.	Newtonian Flow - Flow Direction	31
Figure 4.4.	Newtonian Flow - Area Incident on Surface	32
Figure 5.1.	Rasmussen & He, Configuration 1	37
Figure 5.2.	Configuration 1 Comparison Results	38
Figure 5.3.	Rasmussen & He, Configuration 2	39
Figure 5.4.	Configuration 2 Comparison Results	40
Figure 5.5.	Rasmussen & He, Configuration 3	41
Figure 5.6.	Configuration 3 Comparison Results	42
Figure 5.7.	Hypersonic All-body Configuration	44
Figure 5.8.	HAVOC Model of All-body	44
Figure 5.9.	All-body Results, Mach 2.0, Tangent Wedge & Prandtl-Meyer Methods	49

Figure 5.10. All-body Results, Mach 5.37, Tangent Wedge & Prandtl-Meyer Methods 50
Figure 5.11. All-body Results, Mach 7.38, Tangent Wedge & Prandtl-Meyer Methods 51
Figure 5.12. All-body Results, Mach 10.6, Tangent Wedge & Prandtl-Meyer Methods 52
Figure 5.13. All-body Results, Mach 10.6, Newtonian Method 53
Figure 5.14. Three Mach 8 Waverider Configurations 56
Figure 5.15. Pure Mach 8 Waverider Geometry in HAVOC Code 57
Figure 5.16. Taylor - Maccoll Results of Three Mach 8 Waverider Configurations 57
Figure 5.17. Pressure Distributions Over Lower Surfaces of Two Mach 8 Waverider Configurations 58
Figure 5.18. Effect of Engine on Mach 8 Waverider Performance 58
Figure 5.19. Effect of Fairing on Mach 8 Waverider Performance 60
Figure 5.20. Mach 8 Waverider with Elevators 62
Figure 5.21. Mach 8 Waverider Pitching Moment Characteristics 64
Figure 5.22. Mach 8 Force Coefficients 65
Figure 5.23. Mach 14 Waverider 67
Figure 5.24. On-design Results for Mach 14 Waverider 69
Figure 5.25. Mach 14 Waverider Pitching Moment Characteristics 71
Figure 5.26. Mach 14 Force Coefficients 72

NOMENCLATURE

List of Symbols

A	area
a	speed of sound
CD	total coefficient of drag
CL	total coefficient of lift
Cm	coefficient of pitching moment
Cp	coefficient of pressure
D	drag
dA	incremental area
e	energy
F	force
f	body force
h	enthalpy
L	lift
n	normal axis (Figure 3.6)
p	pressure
$\dot{q}$	heat transfer rate
r	radius
s	entropy
s	streamline axis (Figure 3.6)
s	surface area
t	time

V	velocity
v	volume
θ_c	cone half angle
θ_s	shock angle
ρ	density
Λ	leading edge sweep
ν	Prandtl-Meyer angle
γ	ratio of specific heats

Subscrips

∞	freestream value
0	stagnation value
1	upstream value
2	downstream value
f	friction
n	normal
t	tangential
t	total or stagnation value

Superscripts

$\vec{}$	vector (boldface type also denotes vector)

Acronyms

AOA	Angle Of Attack
AEROSA	AERO Stand Alone
CFD	Computational Fluid Dynamics
FAIRANAL	FAIRing ANALysis
HAVOC	Hypersonic Aircraft Vehicle Optimization Code
WAVRDR	WAVeRiDeR

CHAPTER 1

Introduction

Background

The waverider concept was first introduced by Nonweiler in 1963 [Ref. 1], but the technology of the time, or for the next 20 years, was not capable of producing a hypersonic air-breathing vehicle, so very little research has been done on waverider technology. In recent years, however, interest in waveriders has increased as the possibility of hypersonic cruise flight has become more realistic. Much work has been done on pure waveriders, including optimization, viscous effects, and scramjet integration [Ref. 2 - 4]. In this study, waveriders with fairings are analyzed, both on - design and at various angles of attack.

Waveriders have better aerodynamic characteristics than other hypersonic vehicles because they are designed so that the shock wave emanating from the vehicle stays attached to the waverider's leading edge. This "capturing the shock" has numerous benefits. First of all, the shock separates the flow field on the upper surface from the flow field on the lower surface. There is no spillage of high-pressure flow from the lower surface to the upper surface, so there is no loss of lift near the tip. Second, the uniform flow on the lower surface is ideal for maximizing the efficiency of the scramjet engine inlet. Finally, waveriders incorporate a reverse-design approach. Instead of determining the flow field from a vehicle shape, the

vehicle shape is derived from the known conical flow field. This method speeds up the design process. This reverse-design approach also allows the waverider shape to be created easily from a computer code. The inputs for the computer code are the flow conditions and cone semi-angle. The vehicle shape and the aerodynamic characteristics are the output. All of these special characteristics make the waverider an important concept to consider for hypersonic flight, but more study must be done to determine the feasability of such a concept.

Related Codes

The Systems Analysis Branch at NASA-Ames Research Center is currently involved in the conceptual design and assessment of several hypersonic cruise vehicle configurations. The waverider concept is a likely candidate for speeds ranging from Mach 4 to Mach 14. As part of their study, the Hypersonics group of the Systems Analysis Branch has developed a FORTRAN code that generates and analyzes waverider shapes, aptly called the Waverider code. The Waverider code can generate and analyze any conically derived waverider shape at the on-design condition, using the Taylor-Maccoll equations [Ref. 5] for conical flow.

The inputs for the Waverider code include the freestream Mach number and the generating cone angle. With this input the conical flow field is calculated, including the streamlines and the flow properties. Next the user specified generating curve is used to define the body shape. Since the lower surface follows the streamlines in the conical flow, the surface pressure is already known from the conical flow calculations.

The main limitation of the Waverider code is that it considers only waveriders that are on-design, which means only at one Mach number and an

angle of attack of zero. A waverider will only be on-design during cruise. For the off-design conditions, a different code is required. The Hypersonic Aircraft Vehicle Optimization Code (HAVOC) [Ref. 6], will be used for this purpose. HAVOC uses approximate high speed methods to give a performance assessment of arbitrary vehicle shapes.

The input geometry for HAVOC is based on four equations describing each of four body regions: the upper forebody, the lower forebody, the upper aftbody, and the lower aftbody. This type of input cannot be used to describe a waverider shape, so a need exists to allow HAVOC to accept a point-based input file.

HAVOC is not a Computational Fluid Dynamics (CFD) code. HAVOC separates the geometry into individual panels, and then analyzes each panel independently as if the neighboring panels have no influence on the flow field of the panel being analyzed. This is called a local slope method. HAVOC can perform a complete aerodynamic analysis on a full vehicle geometry in about 30 seconds on a Silicon Graphics Indigo Workstation. A Navier - Stokes code, or even an Euler code, would take many hours on a Cray supercomputer. Of course, accuracy is lost with HAVOC, but at the conceptual design stage, HAVOC is needed only to give approximate results at hypersonic speeds to allow the designer to generate a good conceptual design. A need exists to validate HAVOC, and this is accomplished in this study by comparing HAVOC values on a representative hypersonic vehicle shape with experimental results.

Purpose of Study

The purpose of this study is to:

(1) validate the Waverider code via a comparison with published results.

(2) validate the aerodynamic part of HAVOC via a comparison with experimental results.

(3) develop the waverider concept by incorporating a fairing on the waverider and modifying the Waverider code to analyze the flow around the fairing.

(4) study the effects of a fairing and the engine on aerodynamic performance.

(5) compare the results of the Waverider code and HAVOC on the same waverider configurations.

(6) perform a preliminary aerodynamic analysis and a preliminary stability analysis on a Mach 8 waverider and a Mach 14 waverider.

CHAPTER 2

Waverider Concept

Idealized Cone-derived Waverider

To gain a better understanding of the waverider concept consider the simplest model, the idealized cone-derived waverider [Ref. 7]. A sketch of this model is shown in Figure 2.1. The body is a section of a cone. The wing, which is infinitesimally thin, extends out from the body to the shock that is induced by the conical body. The resulting wing sweep is equal to 90° minus the shock angle. The upper surface is parallel to the freestream, called the freestream surface, and the lower surface, called the compression surface, is completely immersed in the conical flow field. It is this fact that allows the waverider to be analyzed using conical flowfield methods. Since the shock is attached to the wing tips, there is no flow leakage between the freestream and compression surfaces. The flow fields on the upper and lower surfaces are completely independent of each other. The upper surface is subject only to freestream pressure, and the lower surface of the body and the wings are subject to the pressure of the conical flow field.

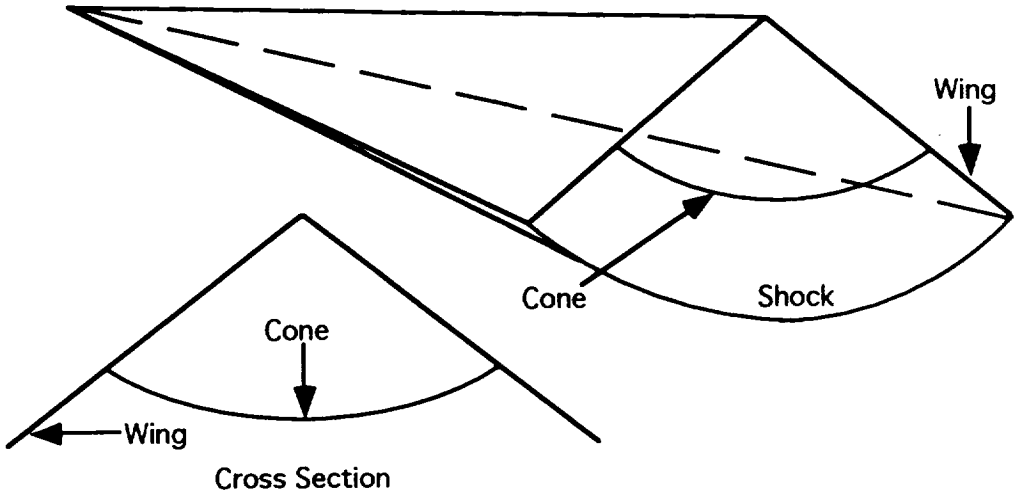

Figure 2.1. Idealized Conical Waverider

General Cone-derived Waverider

Other bodies can be described using the same conical flow field. Although the bodies will not be conical, their shape will be prescribed in such a way that the flow field below the compression surface will be conical and the freestream surface will be parallel to the freestream, thus creating a lift force on the body.

Figure 2.2 [Ref. 7] helps in understanding how a conical wavrider is generated. The waverider can be described by first considering a conical flow field created by an imaginary cone. The leading edge of the waverider is the 3-D intersection of the shock and a generating curve. The generating curve can be any shape. The freestream surface is defined by the locus of streamlines which start at the shock, but follow a freestream path (which are straight lines). The compression surface is defined by the locus of streamlines which start at the shock and follow the paths defined by the conical flow field. These two surfaces form a waverider. The shape of the waverider can be

completely determined if the generating cone angle (θ_C), the Mach number (which determines the shock angle, (θ_S)), and the generating curve are known. If the generating curve is a straight line intersecting with the center of the generating cone, then the resulting waverider will be reduced to the idealized cone-derived waverider.

Other types of waveriders can be created using generating surfaces other than cones to create the flow field, such as power-law bodies. The conical waveriders are the most common and simplest type to date and will be used for this report.

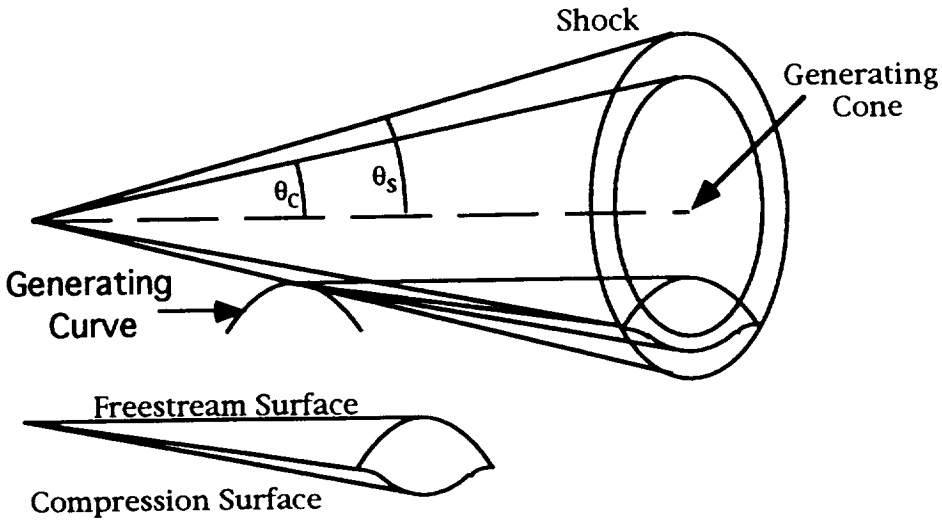

Figure 2.2. General Conical Waverider

CHAPTER 3

Waverider Computer Code

The Waverider code has been developed by the Systems Analysis Branch at NASA - Ames Research Center as a tool for generating and analyzing Waverider shapes. The program first generates the flow field around a cone based upon the user inputs of Mach number and cone angle. The waverider upper surfaces is prescribed by the generating surface, which is also a user input. The lower surface is calculated from the conical flow streamlines, which are known from the Taylor - Maccoll equation [Ref. 8]. If the flow field and the waverider surfaces are known, then the code can assign a pressure coefficient to each panel on the lower surface, depending on where it is in the flow field.

In the following section, applicable concepts of conical flow will first be reviewed, followed by a derivation of the Taylor - Maccoll equation, which is used to solve the conical flow. For this study, the waveriders studied were not "pure" waveriders. Fairings were generated on the back of the waveriders in order to make them more realistic aircraft. Fairing generation will also be discussed in this section, along with a derivation of the Prandtl - Meyer Equations, which are used to analyze the waverider surface in the fairing region.

For calculating friction drag, the Van Driest reference enthalpy model is used [Ref. 9]. The skin friction coefficient (Cf) is a function of Mach

number and the Reynolds number. Boundary layer transition on-set is determined by Reynolds number (based on momentum thickness) and Mach number, and the transition length is equal to the laminar boundary layer length.

Conical Flow

The waverider concepts being considered are generated from conical flow concepts [Ref. 5]. The advantage of using conical flow is that the entire flow field can be determined using the Taylor - Maccoll equation, an ordinary differential equation with only one dependent variable which can be solved numerically.

When a sharp cone is in supersonic flow, an oblique shock wave extends from the vertex, as in Figure 3.1. The shock wave is also conical. A streamline passing through the shock is initially deflected discontinuously, and then curves as it travels downstream approaching a path parallel to the cone surface at infinity. Since the cone is axisymmetric, the flow is also axisymmetric, which means that all flow properties are independent of the cylindrical coordinate ϕ (see Figure 3.2). Therefore a quasi - two dimensional coordinate system as shown in Figure 3.3 can be used.

Since the cone is assumed to extend to infinity, all properties must be constant along the surface. If the pressure, for example, at one point on the surface is different from the pressure at another point, then the pressure at infinity would either be infinity or zero, and this is impossible. We also must assume that flow properties are constant along rays extending from the vertex. These assumptions have been validated experimentally.

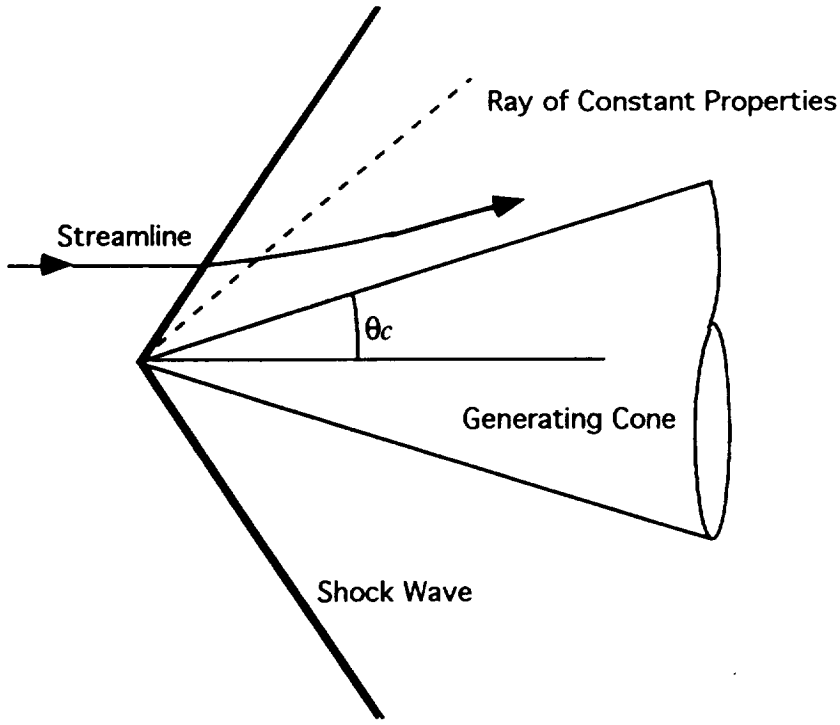

Figure 3.1. Conical Flow field

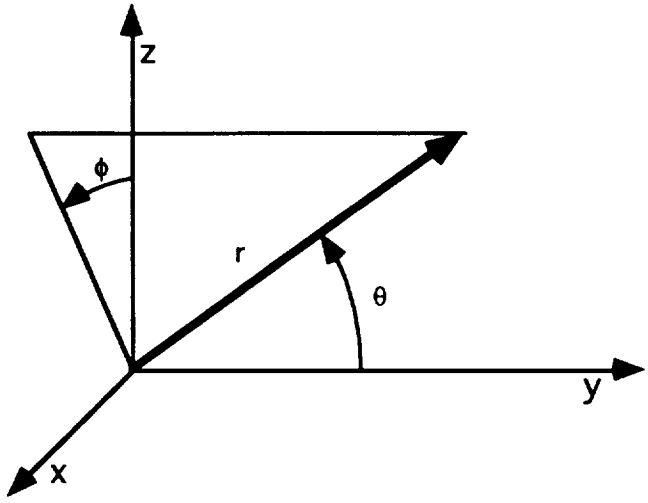

Figure 3.2. Cylindrical Coordinate System

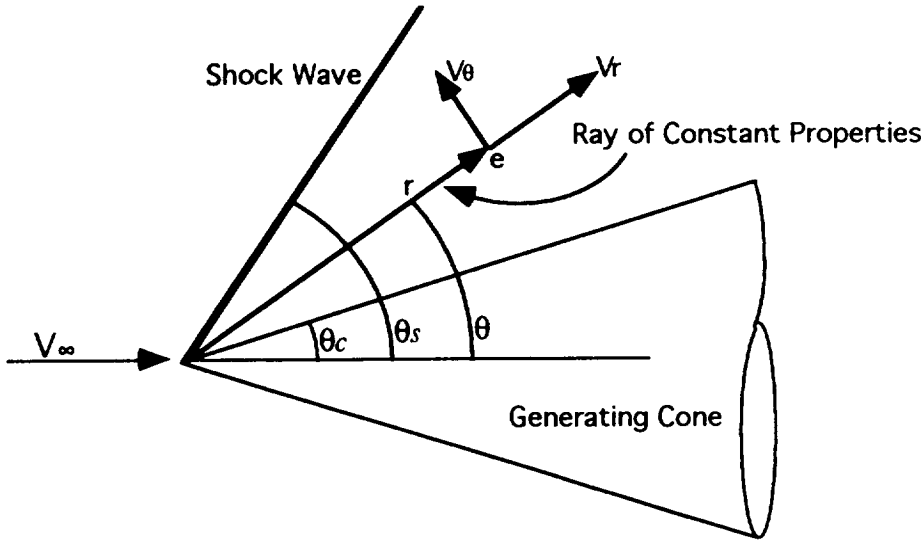

Figure 3.3. Conical Coordinate System

The Taylor - Maccoll Equation

The Taylor - Maccoll Equation can be derived from the conical flow field described above. We will begin with the continuity equation for steady compressible flow, which is

$$\nabla \bullet (\rho \mathbf{V}) = 0 \tag{3.1}$$

The two assumptions for conical flow are that the flow is symmetric about the centerline and that fluid properties are constant along any ray.

$$\frac{\partial}{\partial \Phi} \equiv 0$$

$$\frac{\partial}{\partial r} \equiv 0$$

If the continuity equation is expanded in spherical coordinates and the two above assumptions are applied, the result is

$$2\rho V_r + \rho V_\theta \cot\theta + \rho \frac{2V_\theta}{\partial\theta} + V_\theta \frac{\partial\rho}{\partial\theta} = 0 \tag{3.2}$$

The shock wave in conical flow is straight. Therefore, the increase in entropy behind the shock is the same for all streamlines, or

$$\nabla s = 0$$

For adiabatic and steady flow, the total enthalpy is constant throughout the flow. From Crocco's theorem, if a flow has constant total enthalpy, and constant entropy, then it is irrotational. In spherical coordinates,

$$\nabla x \overline{V} = \frac{1}{r^2 \sin\theta} \begin{vmatrix} e_r & re_\theta & (r\sin\theta)e_\phi \\ \frac{\partial}{\partial r} & \frac{\partial}{\partial\theta} & \frac{\partial}{\partial\phi} \\ V_r & rV_\theta & (r\sin\theta)V_\phi \end{vmatrix} \tag{3.3}$$

If the two assumptions for conical flow are applied, the above equation simplifies to

$$V_\theta = \frac{\partial V_r}{\partial\theta} \tag{3.4}$$

For steady state, irrotational, inviscid flow with no body forces, a simplified version of Euler's equation applies [derived in Ref. 5].

$$dp = -\rho V dV \tag{3.5}$$

where

$$V^2 = V_r^2 + V_\theta^2 \tag{3.6}$$

Since the flow is isentropic, then the speed of sound can be defined as

$$\frac{dp}{d\rho} = a^2$$

Combining these two equations, Euler's equation becomes

$$\frac{d\rho}{\rho} = -\frac{1}{a^2}(V_r dV_r + V_\theta dV_\theta) \tag{3.7}$$

Since the total enthalpy is constant throughout the flow field, we can use the equation of total enthalpy to define a reference velocity, Vmax, the maximum possible (theoretically) obtainable velocity from a fixed reservoir condition. At this velocity, the static temperature and static enthalpy will be zero.

$$h_0 = \text{constant} = h + \frac{V^2}{2} = \frac{V_{max}^2}{2} \tag{3.8}$$

where

$$h = \frac{a^2}{\gamma - 1}$$

Substitute the enthalpy equation into Euler's equation, and the result is Euler's equation for conical flow.

$$\frac{d\rho}{\rho} = -\frac{2}{\gamma - 1}\left(\frac{V_r dV_r + V_\theta dV_\theta}{V_{max}^2 - V_r^2 - V_\theta^2}\right) \tag{3.9}$$

In Equations (3.2), (3.4), and (3.9), there is only one independent variable, θ. All of the partial derivatives with respect to theta can then become ordinary derivatives. Rewrite Equation (3.9)

$$\frac{d\rho}{d\theta} = -\frac{2\rho}{\gamma - 1}\left(\frac{V_r \frac{dV_r}{d\theta} + V_\theta \frac{dV_\theta}{d\theta}}{V_{max}^2 - V_r^2 - V_\theta^2} \right) \tag{3.10}$$

If Equation (3.10) is substituted into Equation (3.2) and changed to ordinary differential form, then the result is

$$\begin{aligned} &\frac{\gamma - 1}{2}\left(V_{max}^2 - V_r^2 - V_\theta^2\right)\left(2V_r + V_\theta \cot\theta + \frac{dV_\theta}{d\theta}\right) \\ &\quad - V_\theta\left(V_r \frac{dV_r}{d\theta} + V_\theta \frac{dV_\theta}{d\theta}\right) = 0 \end{aligned} \tag{3.11}$$

Equation (3.4), in total differential form, is

$$V_\theta = \frac{dV_r}{d\theta} \tag{3.12}$$

therefore,

$$\frac{dV_\theta}{d\theta} = \frac{d^2 V_r}{d\theta^2} \tag{3.13}$$

If we substitute Equation (3.13) into Equation (3.11), then we have the Taylor-Maccoll equation for conical flow.

$$\frac{\gamma-1}{2}\left[V_{max}^2 - V_r^2 - \left(\frac{dV_r}{d\theta}\right)^2\right]\left[2V_r + \frac{dV_r}{d\theta}\cot\theta + \frac{d^2V_r}{d\theta^2}\right] - \frac{dV_r}{d\theta}\left[V_r\frac{dV_r}{d\theta} + \frac{dV_r}{d\theta}\left(\frac{d^2V_r}{d\theta^2}\right)\right] = 0 \tag{3.14}$$

The Taylor - Maccoll equation

The Taylor - Maccoll equation is an ordinary differential equation with only one independent variable, Vr. This equation does not have a closed form solution and must be solved numerically. The Taylor - Maccoll solution yields Vr, and Equation (3.12) determines Vθ. Knowing Vr and Vθ, the Mach numbers throughout the flow field can be found. Since the freestream conditions are given as user inputs, flow properties can be calculated from the Mach number. It follows that the flow properties are functions of θ.

Fairing Generation

Whenever a cone-derived waverider is generated, the aft end of the vehicle is a flat base. A flat base does not create a large drag penalty at high mach numbers. The base drag coefficient [Ref. 10] is modeled as

$$C_p = -\frac{1}{M_\infty^2}$$

However, a base does create enormous drag at transonic and low supersonic speeds. A fairing (see Figure 3.4) helps to reduce the base drag, especially at lower Mach numbers. A well designed fairing recovers as much pressure as

possible, while increasing L/D. The aft fairing also acts as a nozzle expansion surface for the scramjet engine.

There are numerous drawbacks caused by including a fairing. The flow field beyond the longitudinal position at which the fairing starts is no longer conical and the shock is no longer at the leading edge of the wing. The region that includes the fairing does not have as favorable a pressure distribution as the forward aircraft section. The fairing also reduces aircraft volume. Finally, the pressure loss at the rear due to the fairing moves the center of lift forward, which creates a stronger nose-up pitching moment.

To include a fairing in the design, the shape must be created. This is done with a parabolic curve, as shown in Figure 3.5. A parabola is used because it is a common shape for fairings and is relatively simple to prescribe. The user inputs are the fairing starting point, as a percentage of body length, and the departure angle of the parabola. The end of the fairing is the end of the upper surface, plus a user specified base thickness. The two points and the departure angle define a parabola. As the fairing progresses laterally toward the side, the departure angle decreases linearly, and when the fairing is very close to the edge, the fairing becomes linear. This "flattening" of the fairing prevents the bottom surface from penetrating through the top surface.

The flow in the region of the fairing is not conical and the Taylor - Maccoll equation is no longer valid; therefore, the pressure distribution will be calculated using the Prandtl - Meyer flow equations [see Appendix for code that includes fairing generation and flow calculations]. A description of Prandtl-Meyer flow follows.

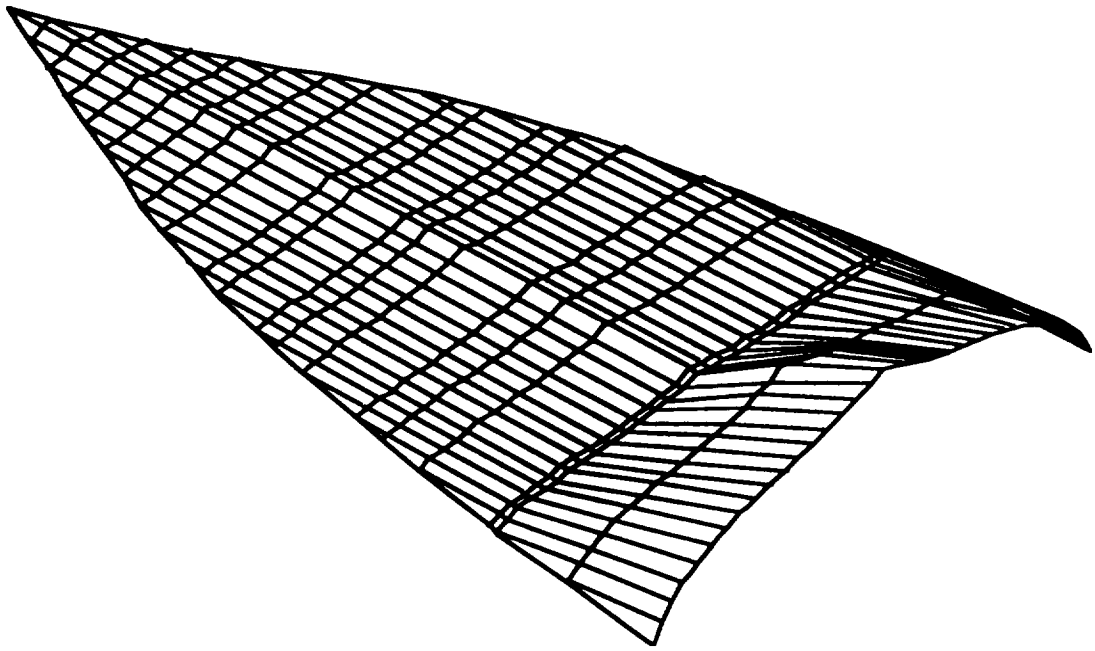

Figure 3.4. Waverider with Fairing(View of Lower Surface)

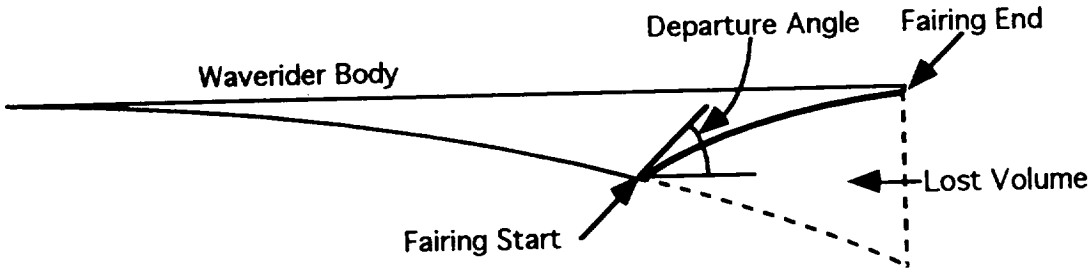

Figure 3.5. Parabolic Curve Describing Fairing

Prandtl-Meyer Flow

The Prandtl-Meyer equations are used to analyze flow that can be assumed to be isentropic, which means that flow is not deflected enough to produce a shock wave [Ref. 11]. Although the fairing is 3-dimensional, The analysis treats it as a series of 2-dimensional longitudinal cuts to simplify the analysis. Figure (3.6) shows a description of the flow. To derive the Prandtl-

Meyer equations we start with the continuity equation for supersonic flow around an airfoil in streamline coordinates, as in Figure (3.6)

$$\frac{\partial(\rho U)}{\partial s}+\rho U\frac{\partial \theta}{\partial n}=0 \tag{3.14}$$

The s-momentum equation

$$\rho U\frac{\partial U}{\partial s}+\frac{\partial p}{\partial s}=0 \tag{3.15}$$

and the n-momentum equation

$$\rho U^2\frac{\partial \theta}{\partial s}+\frac{\partial p}{\partial n}=0 \tag{3.16}$$

The energy equation gives no useful information for isentropic flow, but the equation for the speed of sound for isentropic flow can be used

$$\frac{dp}{d\rho}=a^2$$

When the continuity equation, Equation (3.14), uses the relation for the speed of sound in isentropic flow, it becomes

$$\frac{\partial \rho}{\partial s}\frac{M^2-1}{\partial U^2}+\frac{\partial \theta}{\partial n}=0 \tag{3.17}$$

Combining Equations (3.16) and (3.17), one obtains

$$\partial p + \frac{\rho U^2}{\sqrt{M^2-1}}\partial\theta = 0 \tag{3.18}$$

Euler's equation, for steady, inviscid flow states that

$$d\rho = -\rho U dU$$

Substituting Euler's equation into Equation (3.18), one gets

$$\frac{dU}{U} = \frac{d\theta}{\sqrt{M^2-1}} \tag{3.19}$$

From adiabatic-flow relations for a perfect gas

$$\left(\frac{U}{a_t}\right)^2 = M^2\left(1+\frac{\gamma-1}{2}M^2\right)^{-1} \tag{3.20}$$

where a_t is the speed of sound at the stagnation point. If Equation (3.20) is differentiated, and substituted into Equation (3.19), the result is

$$d\theta = \frac{\sqrt{M^2-1}\,dM^2}{2M^2\left\{1+\left[\frac{\gamma-1}{2}\right]M^2\right\}} \tag{3.21}$$

Integration of Equation (3.21) yields

$$\theta = \nu + \text{ constant of integration}$$

where

$$\nu = \sqrt{\frac{\gamma+1}{\gamma-1}}\arctan\sqrt{\frac{\gamma-1}{\gamma+1}\left(M^2-1\right)} - \arctan\sqrt{M^2-1} \tag{3.22}$$

The Prandtl-Meyer angle, ν, is only a function of the Mach number. The ratio of static to total pressure is given by the equation [Ref. 12]

$$\left(\frac{p}{p_t}\right)^{\frac{\gamma-1}{\gamma}} = \frac{1}{\gamma+1}\left\{1+\cos\left[2\sqrt{\frac{\gamma-1}{\gamma+1}}\left(\nu+\tan^{-1}\sqrt{M^2-1}\right)\right]\right\} \tag{3.23}$$

where p_t is the total pressure. At any given point on the surface of the waverider, if one knows the Mach number, then the Prandtl-Meyer angle can be determined. Adding the deflection angle between two panels to the Prandtl-Meyer angle of the upstream panel, one can obtain the downstream panel's Prandtl-Meyer angle, and then use Equation (3.22) to get the downstream panel's Mach number and pressure ratio. One can get Cp using the definition of the pressure coefficient

$$C_p \equiv \frac{p - p_\infty}{q_\infty}$$

Using this method, the pressure coefficient at every panel in the fairing can be calculated by marching downstream from the beginning of the fairing to the end (which is also the end of the aircraft) at each lateral station. The conditions at the beginning of the fairing, where the forebody expands into the base region, are known from the Taylor - Maccoll equations.

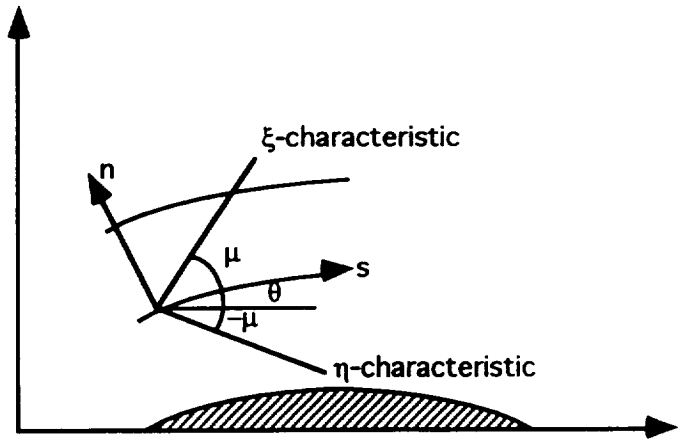

Figure 3.6. Supersonic Flow Around an Airfoil in Streamline Coordinates

CHAPTER 4

HAVOC Computer Code

AEROSA Code

The Hypersonic Aircraft Vehicle Optimization Code (HAVOC) [Ref. 6] is used for conceptual analysis of hypersonic vehicles. The code analyzes the vehicles geometry, propulsion, aerodynamics, structures, and other parameters. For this study, only the aerodynamics portion was needed, so it was separated into a stand-alone version, called AERO Stand Alone (AEROSA). An analysis from AEROSA is equal to an analysis from the aerodynamics portion of HAVOC, and both acronyms are used interchangeably in this report.

The input to the HAVOC code is described analytically by a set of enhanced super ellipses. Four equations describe the upper forebody, lower forebody, upper aftbody, and lower aftbody. Enhanced super ellipses are defined by the equation.

$$\left(\frac{x}{A}\right)^M + \left(\frac{y}{B}\right)^N = 1$$

where: M and N are integers

A and B are real constants

If M and N were both equal to 2, then the equation would reduce to that of a

regular ellipse. This input uses little memory space for storing data, and closely approximates many hypersonic vehicle shapes. However, this type of input does not describe waverider shapes, so the code had to be modified to accept any general body shape as input. The input was modified so that a series of spatial coordinates, one coordinate for each point of the surface, were used to describe the body. This modification was performed by the hypersonics group at NASA - Ames for this study.

The HAVOC code (also the AEROSA code) is not a CFD code. A Navier - Stokes code and other simpler CFD codes solve for the entire flow field using a convergence technique. The HAVOC code solves the flow only on the aircraft surface, analyzing each panel independently and separately. The HAVOC code sacrifices accuracy for speed, which is acceptable for conceptual design when such a wide variety of configurations are being considered. When most design options have been eliminated, a more accurate CFD code will become necessary.

At each panel, the pressure coefficient, Cp, is calculated using one of several approximate methods [Ref. 9]. For panels facing upstream, called impact surfaces, the user can choose either the Tangent Wedge method, the Tangent Cone method, a combination of the Tangent Wedge and Tangent Cone methods, or the Newtonian method. For panels facing downstream, called shadow surfaces, the user may choose the Prandtl-Meyer Expansion method (which was discussed in chapter 3), the Newtonian method, or a High Mach Base Pressure method.

Knowing the pressure coefficient (Cp), the incremental area (dA), and the unit normal at each panel, HAVOC determines values such as lift coefficient (CL), drag coefficient (CD), moment coefficient (Cm), and other related aerodynamic data. Skin friction and heat transfer are computed using a simplified reference enthalpy method [Ref. 9]

For this study, The Tangent Wedge and the Newtonian methods were used for the impact surfaces, because they gave results closest to that of experimental data. The Tangent Wedge method was used as the primary impact method, since the Newtonian method is only used for speeds above Mach 10. For the shadow surfaces, the Prandtl-Meyer Expansion method is used for most cases, while the Newtonian method is also used for speeds above Mach 10. The High Mach Base Pressure method is not used because it's did not perform as well as the other methods when compared to experimental data. The Prandtl-Meyer theory has already been discussed in Chapter 3. A discussion of the Tangent Wedge theory and the Newtonian theory follows.

Tangent Wedge Theory

The Tangent Wedge theory is based on the two-dimensional oblique shock relations [Ref. 5]. It assumes that, at each panel on the hypersonic body, the Cp is the same as that on a 2-d wedge whose inclination angle is the same as that of the panel. The panel's inclination angle to the free stream is known from the body's geometry and angle of attack. To find the Cp of the corresponding wedge, one needs only use the oblique shock relations.

A common example of an oblique shock is a 2-d wedge, as shown in Figure 4.1. The flow ahead the shock is the free stream flow. As the flow crosses the shock, it is deflected to an angle parallel to the surface of the wedge. Figure 4.2 shows a breakdown of the flow into its normal and tangential components as it crosses the shock. Lines *a* through *f* represent a control volume of air passing through the shock. The continuity equation in integral form is

$$-\iint_S \rho \mathbf{V} \bullet d\mathbf{S} = \frac{\partial}{\partial t} \iiint_V \rho dV$$

The flow is assumed to be steady, so the temporal term drops out. Surfaces *b*, *c*, *e*, and *f* are parallel to the velocity, so there is no flow across these surfaces. w_1 and w_2 are tangent to surfaces *a* and *d*. The continuity equation, when applied to the control volume in Figure 4.2 with the above conditions, becomes

$$\rho_1 u_1 A_1 = \rho_2 u_2 A_2$$

A_1 and A_2 are the areas of surfaces a and d, and are equal, so

$$\rho_1 u_1 = \rho_2 u_2 \tag{4.1}$$

The integral form of the momentum equation for inviscid flow is

$$\iint_S (\rho \mathbf{V} \bullet d\mathbf{S})\mathbf{V} + \iiint_V \frac{\partial(\rho \mathbf{V})}{\partial t} dV = \iiint_V \rho \mathbf{f} dV - \iint_S p d\mathbf{S}$$

The assumptions of steady flow and no body forces eliminates both volume integrals. The momentum equation is easiest to analyze when resolved into components tangential and normal to the shock wave. For the tangential component, the pressure integral is zero, because the tangential component of pdS is zero on surfaces *a* and *d* . Also, the pdS component on surface *b* cancels that on *f*, and the pdS component on surface *c* cancels that on *e*. The resulting momentum equation in the tangential direction is

$$(-\rho_1 u_1) w_1 + (\rho_2 u_2) w_2 = 0 \tag{4.2}$$

Substituting Equation. (4.1) into Equation. (4.2), we obtain

$$w_1 = w_2$$

From this we can conclude that the flow tangential to an oblique shock does not change. This is an important result, because the normal component of the flow sees the oblique shock as merely a normal shock. The following equations will show this. The normal component of the momentum equation is

$$(-\rho_1 u_1) u_1 + (\rho_2 u_2) u_2 = -(-p_1 + p_2)$$

or

$$p_1 + \rho_1 u_1^2 = p_2 + \rho_2 u_2^2 \tag{4.3}$$

The integral form of the energy equation, without the friction and time derivative terms, is

$$\iiint_V \dot{q}\rho dV - \oiint_S p\mathbf{V} \bullet d\mathbf{S} = \oiint_S \rho\left(e + \frac{V^2}{2}\right)\mathbf{V} \bullet d\mathbf{S} \tag{4.4}$$

Since there is no heat addition, the first term is zero. Applied to the normal component of flow, Equation (4.4) becomes

$$-(-p_1 u_1 + p_2 u_2) = -\rho_1\left(e_1 + \frac{V_1^2}{2}\right)u_1 + \rho_2\left(e_2 + \frac{V_2^2}{2}\right)u_2$$

or

$$\left(h_1+\frac{V_1^2}{2}\right)\rho_1 u_1=\left(h_2+\frac{V_2^2}{2}\right)\rho_2 u_2 \tag{4.5}$$

Dividing Equation. (4.5) by (4.1),

$$h_1+\frac{V_1^2}{2}=h_2+\frac{V_2^2}{2} \tag{4.6}$$

We know that V2 = u2 + w2, and that w1 = w2

$$V_1^2-V_2^2=\left(u_1^2+w_1^2\right)-\left(u_2^2+w_2^2\right)=u_1^2-u_2^2$$

So Equation (4.6) becomes

$$h_1+\frac{u_1^2}{2}=h_2+\frac{u_2^2}{2} \tag{4.7}$$

Equations (4.1), (4.3), and (4.7) are all identical in form to the continuity, momentum, and energy equations for a normal shock. The only difference is that in an oblique shock, there is also a tangential component, which is not changed. In the oblique shock, the relations depend solely on the flow normal to the shock. All of the relations developed for the normal shock can be derived for the flow normal to the oblique shock in exactly the same manner. From the geometry,

$$M_{n1}=M_1\sin\beta$$

The following relations assume a calorically perfect gas,

$$\frac{p_2}{p_1} = 1 + \frac{2\gamma}{\gamma+1}\left(M_{n_1}^2 - 1\right) \tag{4.8}$$

$$\frac{\rho_2}{\rho_1} = \frac{(\gamma+1)M_{n_1}^2}{(\gamma+1)M_{n_1}^2 + 2}$$

$$\frac{T_2}{T_1} = \frac{p_2}{p_1}\frac{\rho_1}{\rho_2}$$

$$M_{n_2}^2 = \frac{M_{n_1}^2 + [2/\gamma - 1]}{[2/\gamma - 1]M_{n_1}^2 - 1}$$

Also from the geometry in Figure (4.2),

$$M_2 = \frac{M_{n_2}}{\sin(\beta - \theta)}$$

We now have all the information necessary to calculate the pressure coefficient using the Tangent Wedge method. Note that the flow properties behind the shock are constant along any ray throughout the flow field, including the surface.

The Tangent Wedge method and the Tangent Cone methods are only approximate. They cannot be derived from a flow model. The reason these methods are used is because they are straightforward and turn out to be quite accurate for hypersonic speeds, due mainly to the thin shape of most hypersonic vehicles.

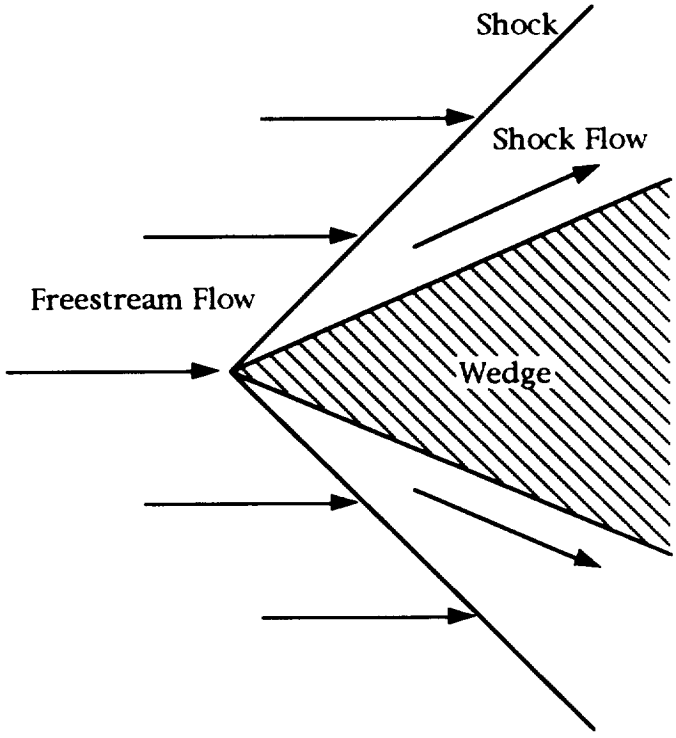

Figure 4.1. Supersonic Flow Past a Wedge

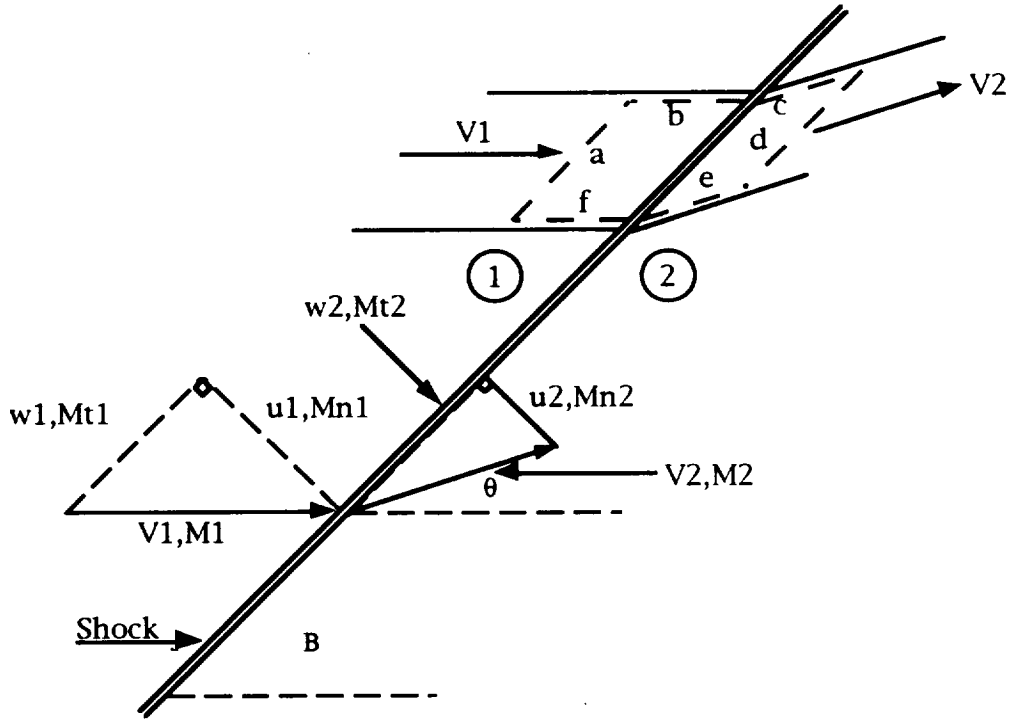

Figure 4.2. Flow Crossing Shock

Newtonian Theory

Isaac Newton proposed that the force on a surface is equal to the loss of momentum of the flow normal to the surface [Ref. 13]. If a stream of flow impacts upon a surface, the momentum normal to the surface is transferred to the surface, and the momentum tangential to the surface will remain unchanged. Therefore, after the flow strikes the surface, it will turn parallel to the surface, as shown in Figure 4.3 [Ref. 5]. The change in normal velocity is $V_\infty \sin\theta$, and the mass flux of particles incident (see Figure 4.4) on the surface is $\rho V_\infty A \sin\theta$. From Newton's 2nd law, force is equal to the time rate of change of momentum, which is equal to the mass flux times the velocity change. In equation form, this is

$$F = \text{mass flux} * \text{velocity change} = (\rho V_\infty A \sin\theta)(V_\infty \sin\theta) = \rho V_\infty^2 A \sin^2\theta$$

Pressure is Force per unit area

$$\frac{F}{A} = \rho V_\infty^2 \sin^2\theta$$

Newton assumed that the stream of particles hitting the surface did not interact with each other, and did not have any random motion. Since static pressure is due to the random motion of particles, and since Newton's equation does not consider this, the value of F/A must be the pressure difference above the static pressure, or $F/A = p - p_\infty$. Using the definition of Cp, we have

$$C_p \equiv \frac{p - p_\infty}{\frac{1}{2}\rho V_\infty^2} = \frac{\rho V_\infty^2 \sin^2\theta}{\frac{1}{2}\rho V_\infty^2}$$

$$C_p = 2\sin^2\theta \tag{4.9}$$

Equation (4.9) is the Newtonian equation. Obviously, it can be seen that many of Newton's assumptions were incorrect. Particles do have random motion, which is the source of static pressure. Also the momentum normal to the surface is not completely transferred to the surface, as Newton suggested. Fortunately, for high speed flow, as Mach number increase, and the shock gets closer to the body surface, Flow does approach the behavior as Newton suggested. In fact, the exact shock wave relations approach the Newtonian result as the ratio of specific heats, γ, approaches unity. γ approaches unity for dissociating and ionizing flow, which occurs at high speed. This result can be seen by substituting $\gamma = 1$ and $M_1 = \infty$ into Equation (4.8). The result is the Newtonian equation.

In Newtonian flow in the shadow region, stream particles cannot curl around the body and impact upon the shoadow surface, which means that no pressure can be felt. Therefore the model assumes that Cp = 0 for all shadow surfaces. Again, this is accurate as $M \rightarrow \infty$.

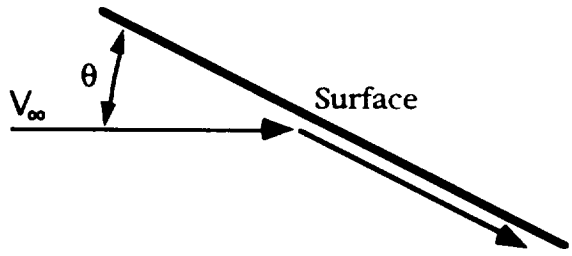

Figure 4.3. Newtonian Flow - Flow Direction

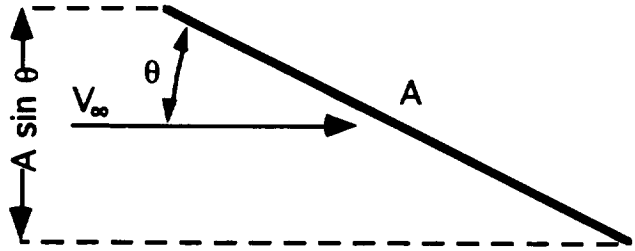

Figure 4.4. Newtonian Flow - Area Incident on Surface

CHAPTER 5

Results & Discussion

The first two sections of this chapter are devoted to validation of the Waverider code and HAVOC. The last two sections present the results of analyzing Mach 8 and Mach 14 waveriders generated from the Waverider code. Only the Mach 8 waverider is used to show the effect of a fairing and an engine shape on the vehicle's performance. Both the Mach 8 and the Mach 14 Waverider are used to compare analysis methods, and both are used for an off-design analysis in HAVOC.

Comparison of Three Waveriders with Published Configurations

In order to validate the aerodynamic performance values generated by the Waverider code, the results were compared against several waverider configurations developed by Rasmussen and He [Ref. 7]. Rasmussen and He published tabulated data of several waverider configurations. The tabulated data included Reynold's number, geometric length and volume ratios, CL, CD (both pressure and friction drag), and L/D[1]. Three different configurations were chosen, each representing different possible types of configurations.

---

1 The L/D ratios presented from the Waverider code are all at 0° AOA (cruise condition). Many high speed aircraft are presented with maximum L/D. This should be kept in mind when comparing performance numbers.

The published waveriders are all "pure" waverider configurations, which means that there is no engine or ramps, and no fairing. The conical flow is maintained throughout the lower surface of the waverider, and the aft end of the vehicle is a flat base. All three configurations are Mach 10 waveriders. The generating cone and the generating curve were variables used to determine the different configurations.

Several changes were made to the Waverider code to make the results comparable with the published results. First of all, and most important, is that Rasmussen and He do not account for base drag in their calculations. A waverider could very possibly be only the forebody of a complete vehicle. If this is the case, then the base drag will be accounted for by the rear section of the vehicle. Also, Rasmussen and He do not account for leading edge pressure forces, which are present because the leading edge has a finite radius, and therefore has a higher pressure than a sharp corner. This higher pressure increases the total drag on the vehicle. The leading edge pressure also increases the lift a small amount, but the overall effect is to lower the L/D. Because of these two factors, the performance of the published vehicles is somewhat optimistic. Still, they are suitable for comparison purposes.

Rasmussen and He use hypersonic small-disturbance theory for inviscid analysis, with a laminar boundary-layer theory to account for the viscous effects. The Waverider code uses the Taylor - Maccoll equation for conical flow, with a boundary-layer theory that accounts for laminar, transition, and turbulent effects.

All three configurations have a length of 150 ft., a Mach number of 10 at an altitude of 150,000 ft., and a dynamic pressure of 198.9 psf. The Reynolds number based on vehicle length is 15.9 million. Since they assume a laminar boundary layer, Rasmussen and He used a Reynolds number of 10 million.

Configuration 1

Configuration 1 is shown in Figure 5.1, and has a flat top. It is the flattest of the three configurations, and also has the widest base. Shown in Figure 5.2 are the lift coefficients (CL), drag coefficients (CD_p and CD_f), and L/D values. CL and CD_p values differ by only 2% and are in excellent agreement. Pressure L/D (L/D,p) values (L/D,p is CL divided by CD_p) are also very similar. The only real discrepancy is the friction drag coefficient (CD_f). Rasmussen and He predict a lower CD_f than does the Waverider code. Because they assumed a laminar boundary layer model which resulted in lower CD_f values than a model that also includes transition and turbulent boundary layers, Rasmussen & He have a higher L/D_{total} than the Waverider code. L/D_{total} is CL divided by the total CD.

Configuration 2

Configuration 2, shown in Figure 5.3, was designed to have a free stream trailing edge with zero slope at the shock. These types of waveriders tend to have a higher concentration of volume in the center of the body. The results for configuration 2, shown in Figure 5.4, are very similar to those for configuration 1. CL, CD_p, and L/D,p are all in excellent agreement. CD_f is lower for Rasmussen and He, and L/D_{total} is therefore higher.

Configuration 3

Configuration 3, shown in Figure 5.5, has a trailing edge with both a maximum and a minimum. This is called a reflexed trailing edge. These types of waveriders are generally flared near the base. Most waveriders tend to be longitudinally statically unstable, because of the high forebody pressure. Reflexed trailing edge waveriders, with the extra aft surface area, tend to be

less unstable than other waveriders. Also, the reflexed waveriders more easily accommodate flaps than most other waverider shapes. The results for Configuration 3, shown in Figure 5.6, were very similar to those of Configurations 1 and 2.

Summary

We can conclude that the Waverider code does compare favorably with the published results of Rasmussen and He. The largest discrepancy was in the prediction of CD_f. The Waverider code friction drag results were consistently higher than the published results because Rasmussen and He use a laminar boundary layer model and the Waverider code uses a laminar / transition / turbulent model.

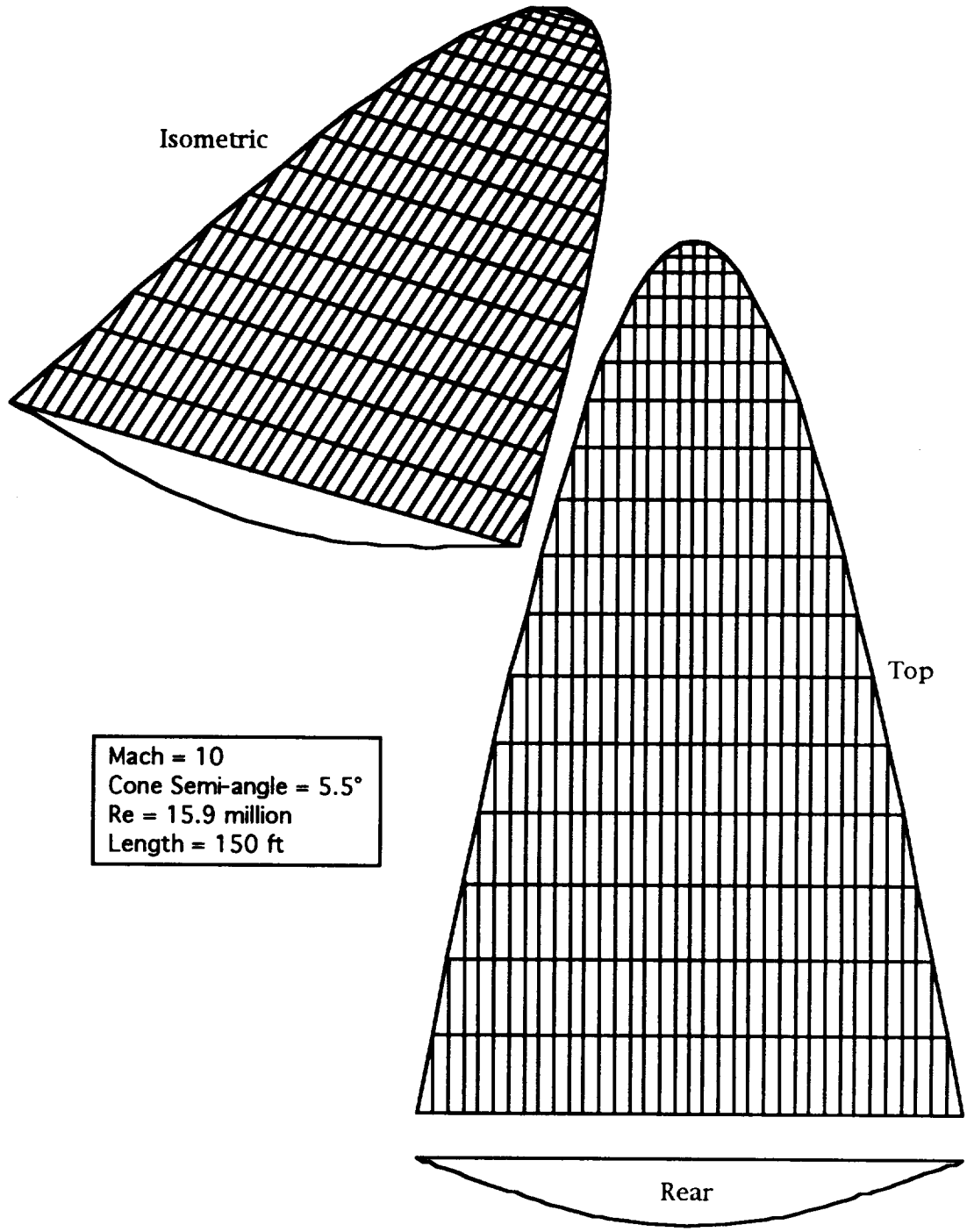

Figure 5.1. Rasmussen & He, Configuration 1

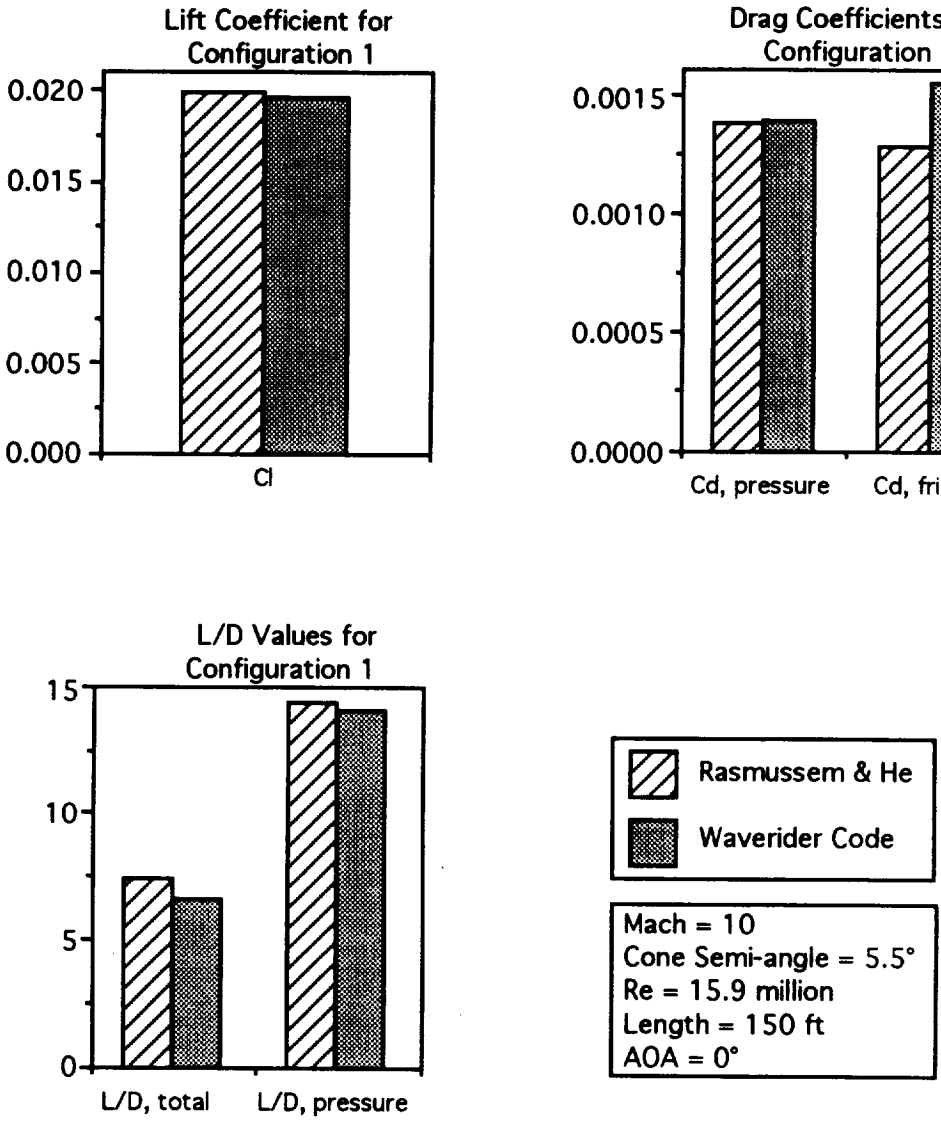

Figure 5.2. Configuration 1 Comparison Results

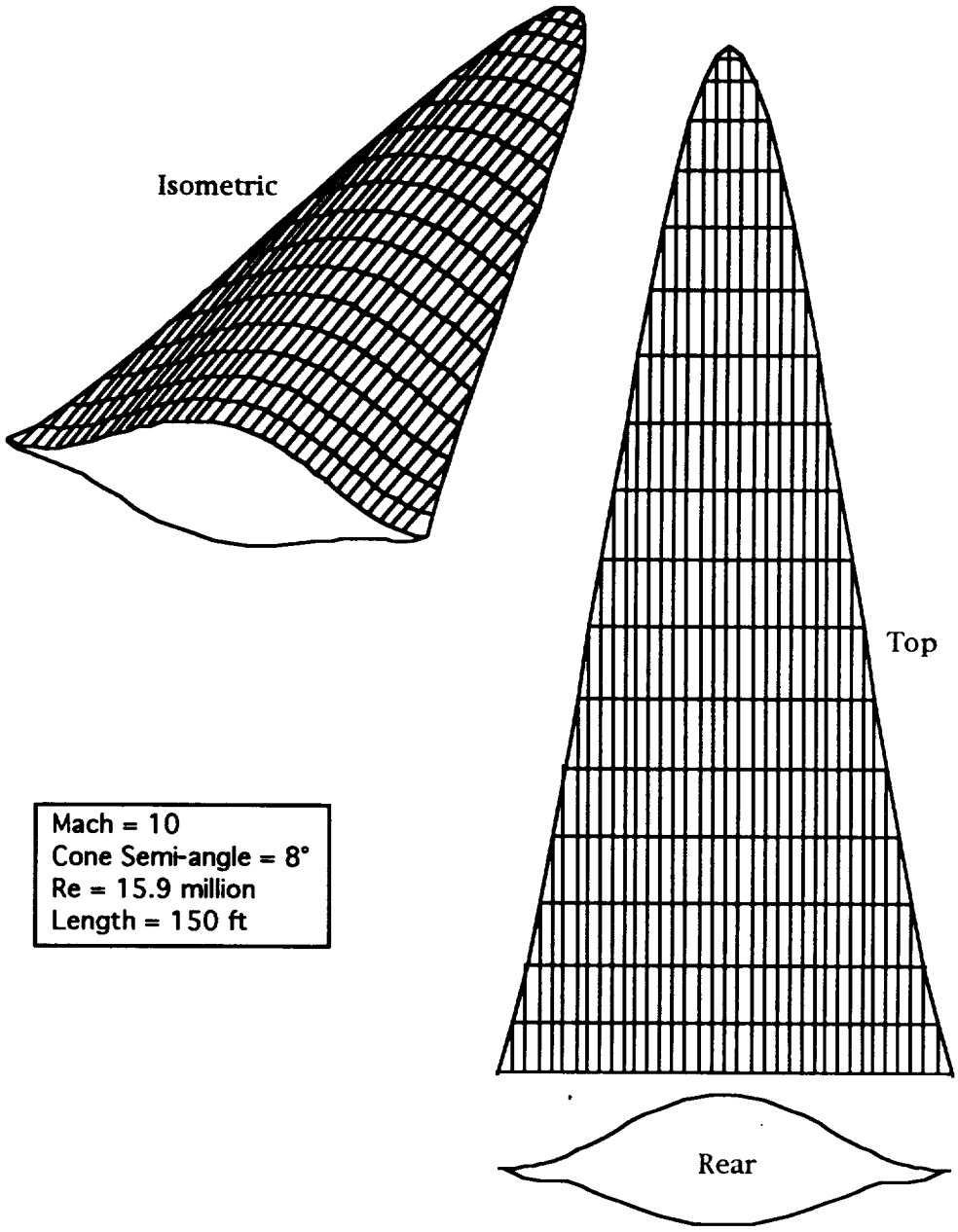

Figure 5.3. Rasmussen & He, Configuration 2

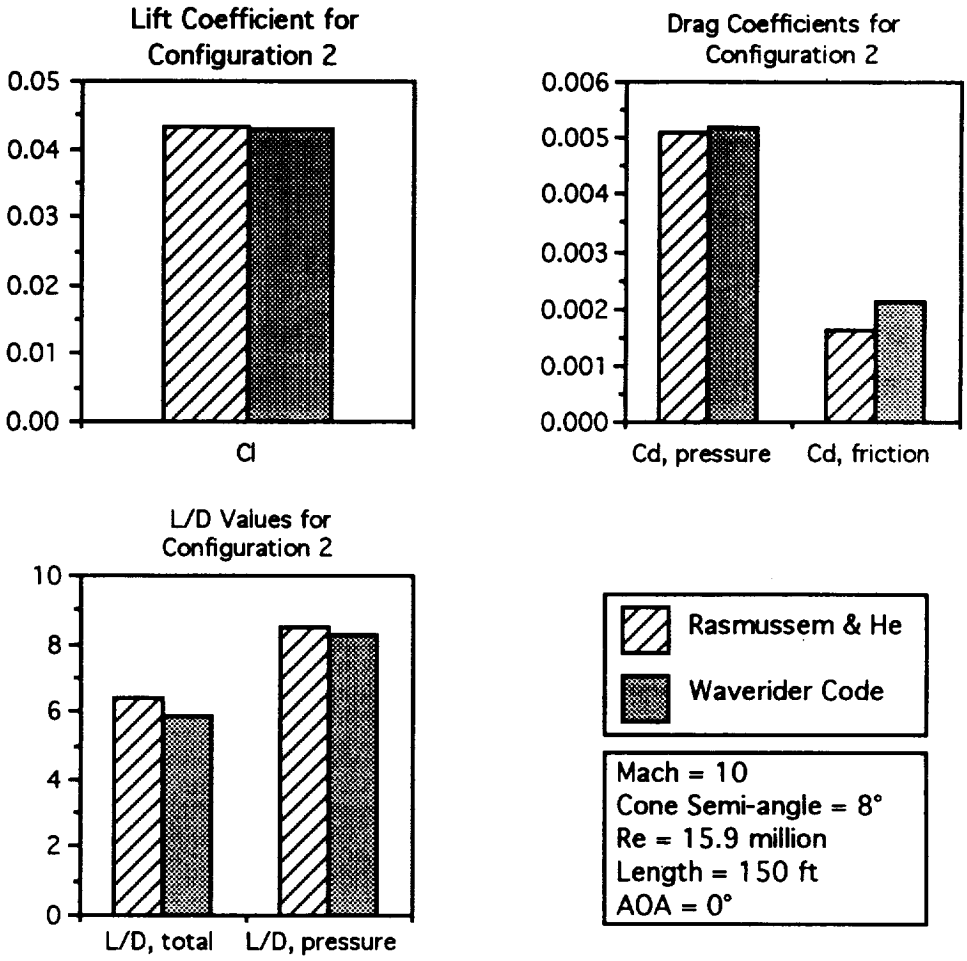

Figure 5.4. Configuration 2 Comparison Results

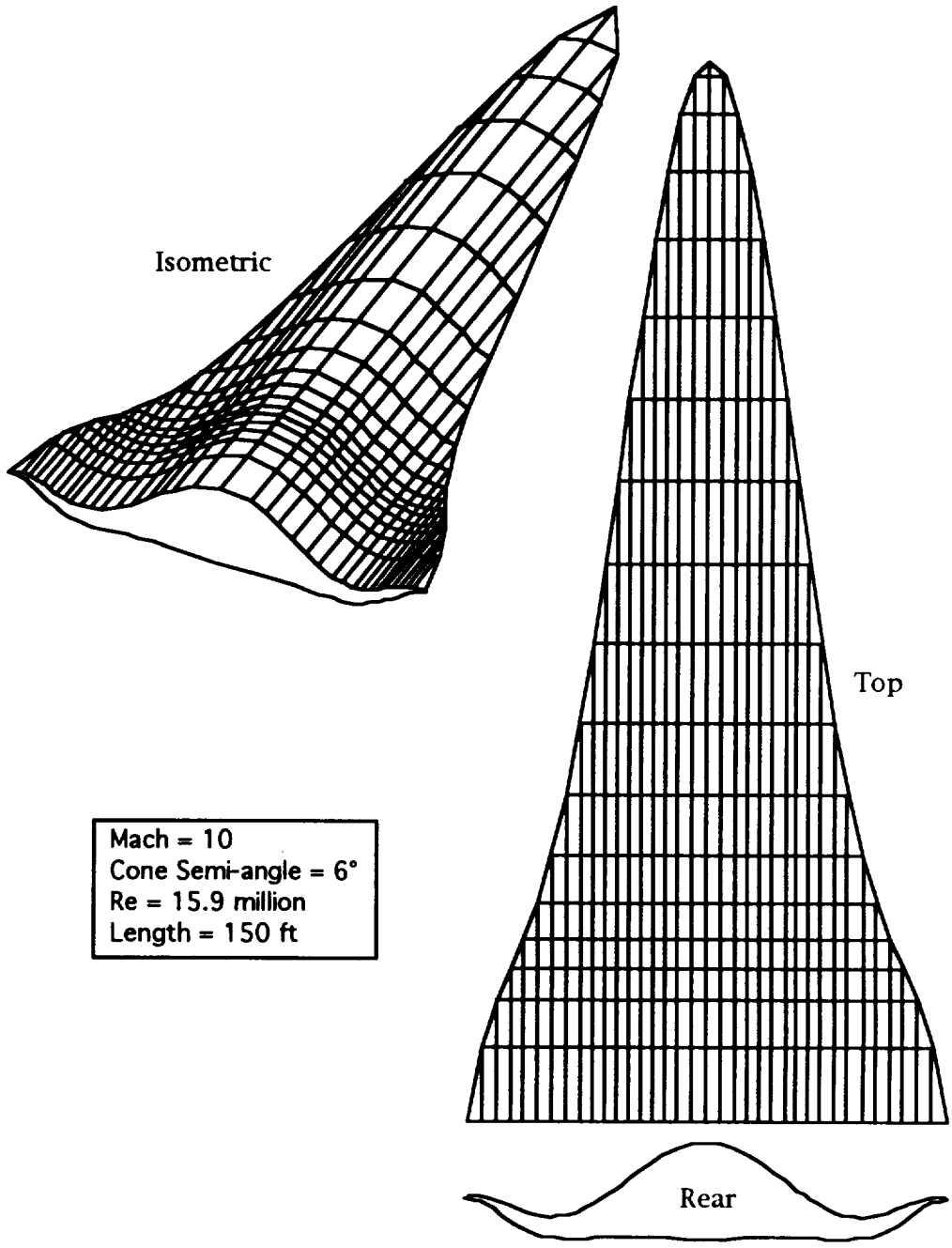

Figure 5.5. Rasmussen & He, Configuration 3

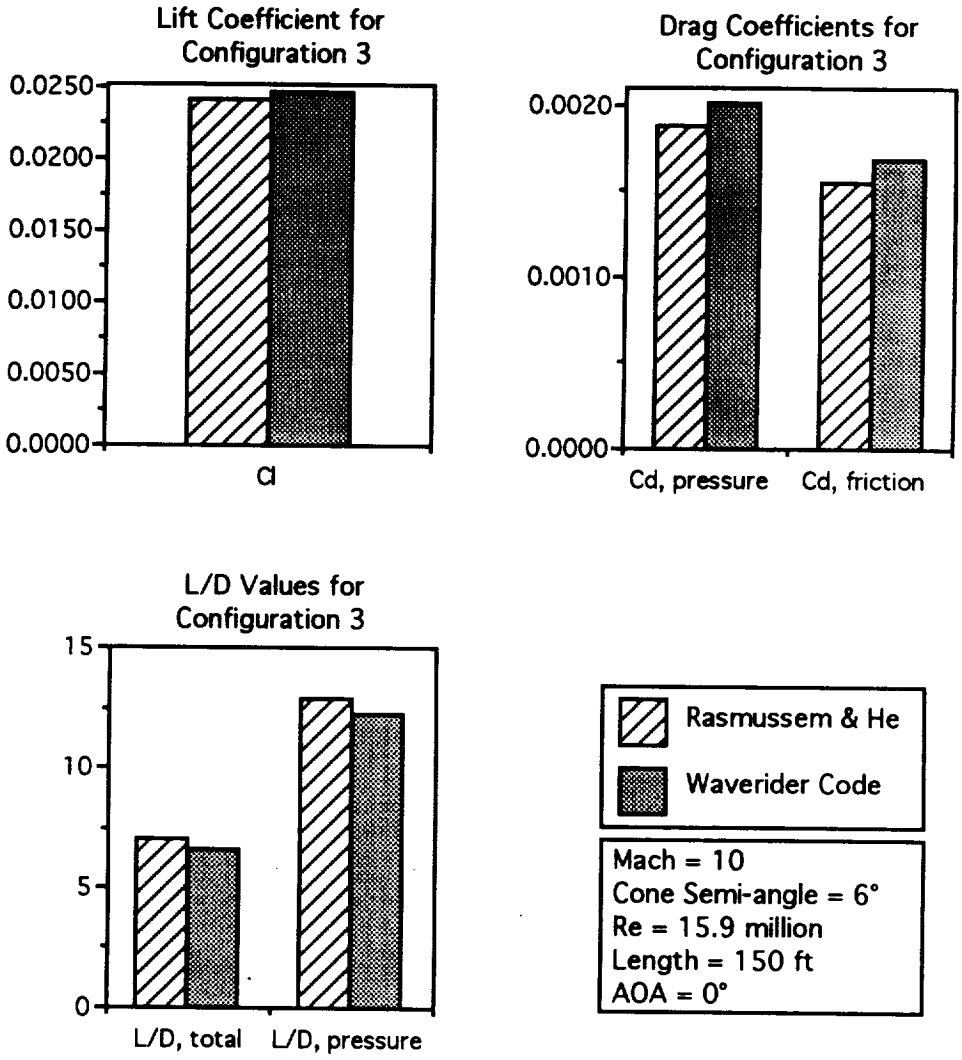

Figure 5.6. Configuration 3 Comparison Results

Comparison of HAVOC Code with Experimental Results

The All-Body Hypersonic Test Model

During the 1960's and 1970's, numerous wind tunnel tests were performed by Nelms and Thomas [Ref. 14] on a test model to generate a large data base of test results for a hypersonic vehicle. The acquired results have been used extensively for hypersonic code validation, and will again be used as a validation for HAVOC (and AEROSA).

The test model, shown in Figure 5.7, is an all-body shape (It is not a waverider). The all-body model does have attachable canards, vertical tails, and horizontal tails which are all shown in the Figure 5.7. For comparison with HAVOC, the all-body was used without any of the attachable control surfaces. The all-body shape can be defined by just three cross sections; the nose (which is a point), the maximum cross section (which is an ellipse located at 2/3 body length), and the rear (which is a line). Figure 5.8 shows a wire frame drawing of the all-body model used.

The aerodynamic characteristics compared are CL, CD, L/D, and Cm. Wind tunnel tests were performed at Mach numbers from 0.65 to 10.6. The four test points used for comparison are Mach 2.0, Mach 5.37, Mach 7.38, and Mach 10.6. At all four test points, the Tangent Wedge method was used for the impact surfaces, and the Prandtl-Meyer relations were used for all the shadow surfaces. At Mach 10.6 the Newtonian method was also used. For all Cm calculations, the Center of Gravity was chosen to be 55% of the body length.

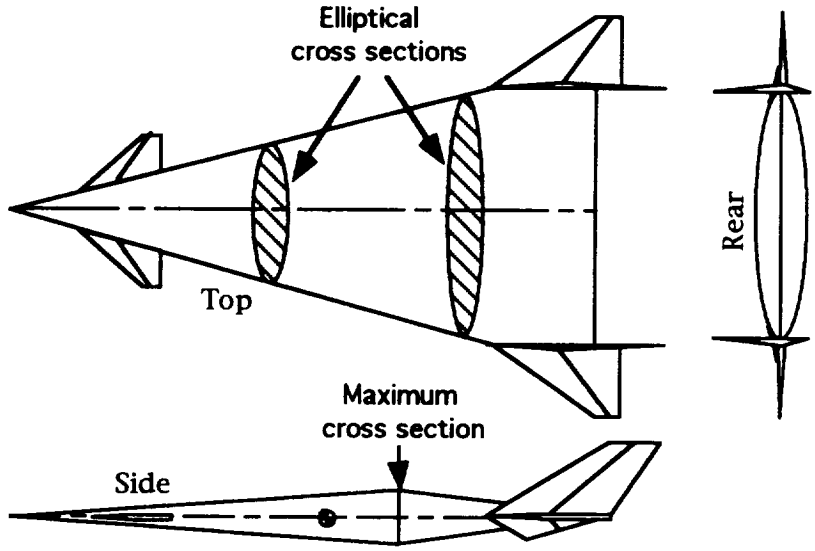

Figure 5.7. Hypersonic All-body Configuration

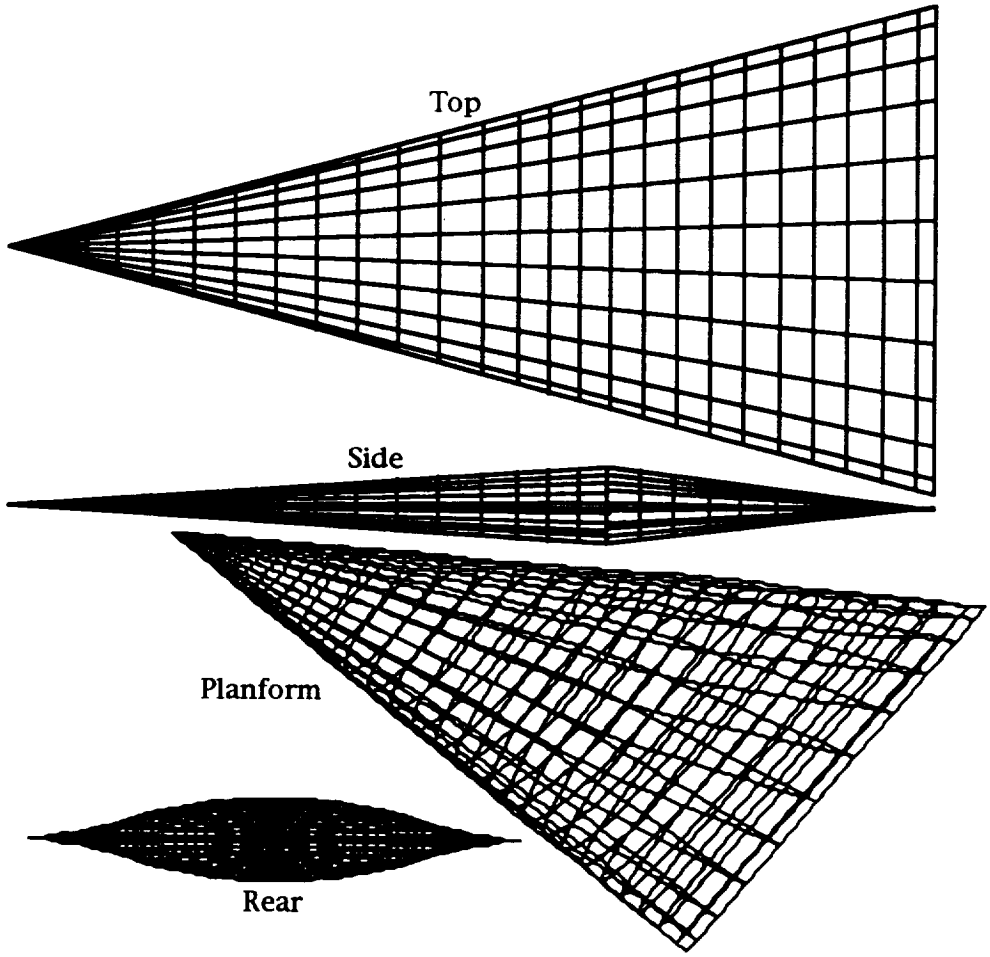

Figure 5.8. HAVOC Model of All-body

Mach 2.0 Results

At Mach 2.0, using the Tangent Wedge and the Prandtl - Meyer methods, HAVOC overestimates the absolute value of both the lift and drag coefficients through all angles of attack, as shown in Figure 5.9. Cm is more negative theoretically than experimentally. Note that the experimental Cm is not zero at zero angle of attack as it should be for a symmetric vehicle. Since both the CL and CD values were off, it is fortuitous that the L/D values compare favorably. The main reason for the discrepancy in CL and CD is that HAVOC does not account for leading edge suction, a phenomenon that occurs when the local Mach number is subsonic and the leading edge has a finite radius. If the flow becomes subsonic over the leading edge, it can sense the pressure gradient ahead and adjust its flow path. This adjustment causes the flow to accelerate, lowering the static pressure on the leading edge, therefore decreasing the wave drag and lift.

The critical Mach number is the point at which the Mach number normal to the leading edge of the vehicle is equal to one. Above the critical Mach number, leading edge suction no longer occurs, and the Tangent Wedge method should be more accurate. The critical Mach number can be determined from the leading edge sweep

$$M_{critical} = \frac{1}{\cos(\Lambda_{LE})}$$

For the All-body, the leading edge sweep = 75°, so $M_{critical}$ = 3.86. From this it is expected that leading edge suction will not occur at the next test point, Mach 5.37, or at higher Mach numbers.

Mach 5.37 Results

At Mach 5.37, the HAVOC code performed much better, as shown in Figure 5.10. CL was almost exactly predicted, and CD predictions were slightly high, but accurate within 10%. L/D values were also accurate within 10%. Cm values are not as accurate, but they do show the proper trends. At Mach 5.37, the flow is completely supersonic, and leading edge suction no longer occurs. Again note that the experimental values of Cm are not zero at zero AOA, and the results are not symmetric between -2 and +2 degrees.

The values of CL and CD are predicted accurately, but Cm values are less negative than experimental values. Higher pressures are predicted on the forebody and lower pressures are predicted on the aftbody. This pressure distribution would result in very little net change in CL and CD, but would cause a less negative Cm.

Mach 7.38 Results

The results at Mach 7.38, shown in Figure 5.11, are very similar to those at Mach 5.37. CL and CD values are accurately predicted. L/D values are also in agreement. The predicted values of Cm are not accurate. At higher angles of attack, the experimental results indicate mostly negative values of Cm while HAVOC predicts positive values. In addition, the HAVOC prediction of Cm values agree with experimental results for angles of attack as low as -2.5°, but at positive angles of attack, there is disagreement above 1°. At high angles of attack, the lower rear surface will have a large effect on Cm, because the vehicle is widest at the rear and that area has a long moment arm. In the experiment, slightly higher pressures occur on the lower rear surface than HAVOC predicts, and this causes HAVOC's Cm values to be more positive than the experimental results.

Mach 10.6 Results

At Mach 10.6, the Tangent Wedge and Prandtl-Meyer results, shown in Figure 5.12, are again accurate, although they are not as accurate as the results at Mach 5.37 and 7.38. CL, CD, and L/D are all slightly over predicted. The positive experimental Cm values increase at this higher speed, but HAVOC did not predict this trend very well.

The Newtonian method theory is most accurate at high Mach numbers, and was also used at Mach 10.6. CL, CD, and L/D are all in excellent agreement with the experimental values, as shown in Figure 5.13, and the Cm values are within 25% and display the same trend as above.

Summary

The results presented show that the HAVOC approximate hypersonic methods are very satisfactory for predicting CL, CD and L/D for conceptual vehicle designs, but only moderately satisfactory for predicting Cm. Although these methods would not be accurate enough for a preliminary or detailed design, that is not what HAVOC is intended to be used for. HAVOC can now be used to predict aerodynamic characteristics for conceptual designs of waverider shapes at off - design conditions. The results of this analysis are presented later on in this chapter.

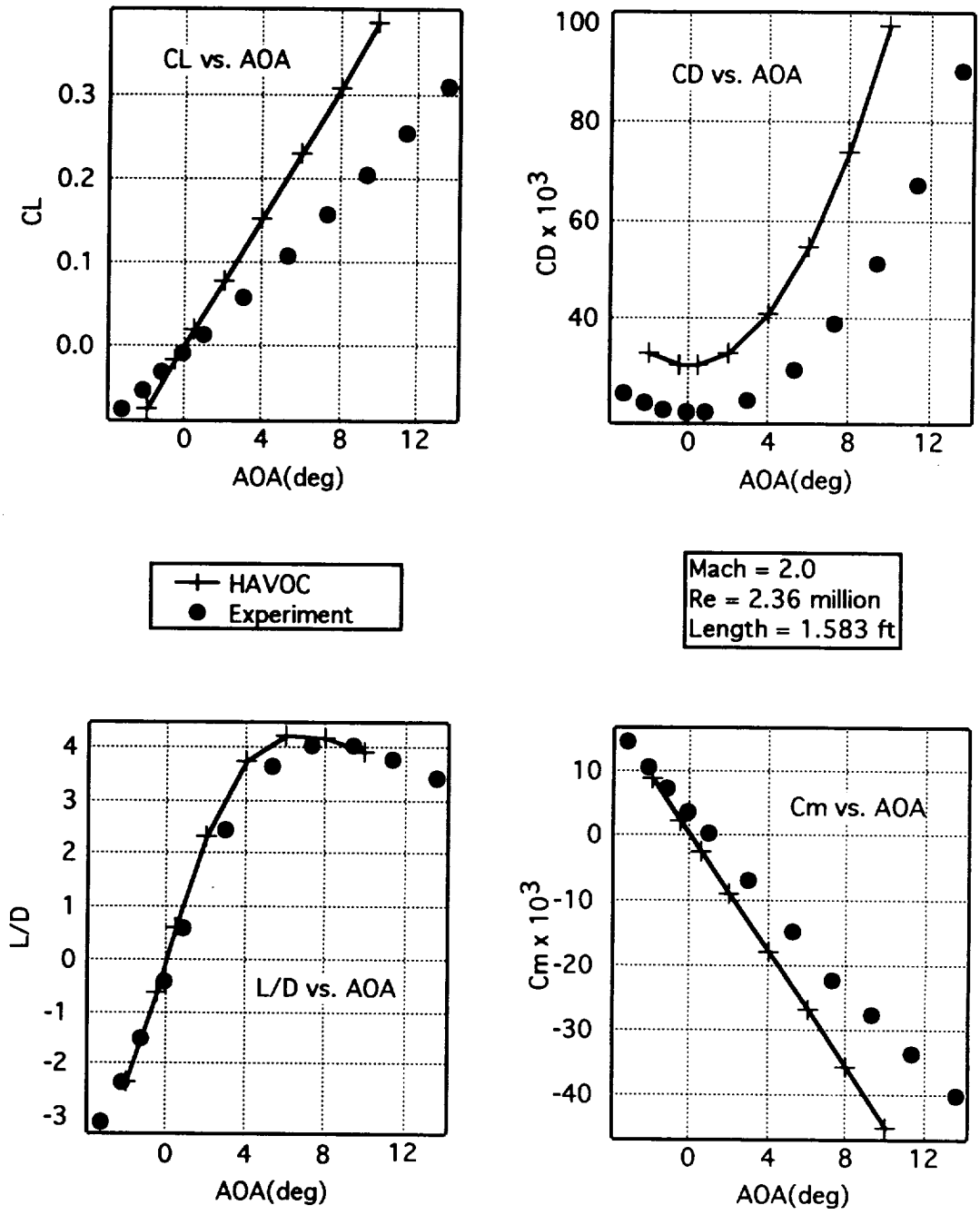

Figure 5.9. All-body Results, Mach 2.0, Tangent Wedge & Prandtl-Meyer Methods

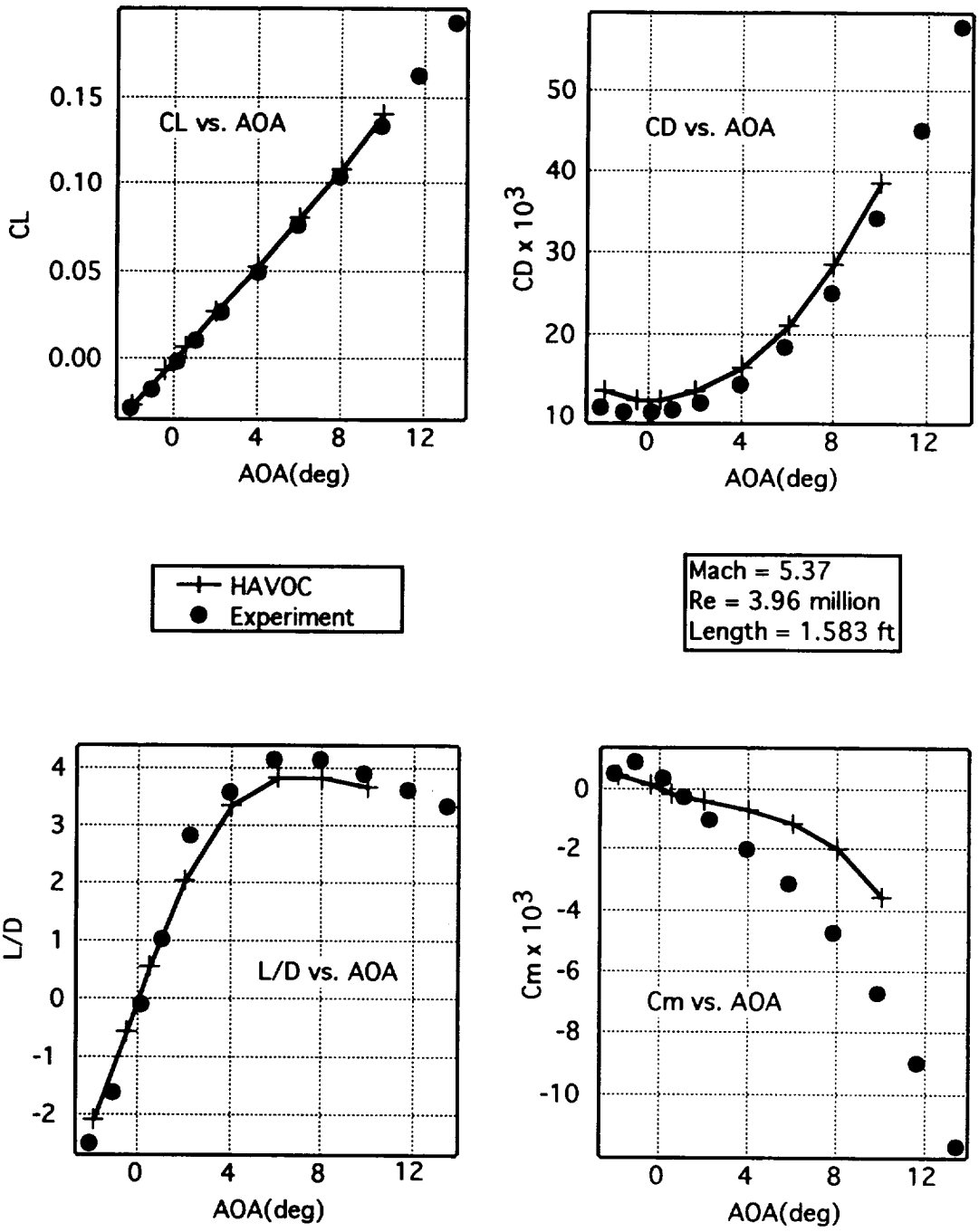

Figure 5.10. All-body Results, Mach 5.37, Tangent Wedge & Prandtl-Meyer Methods

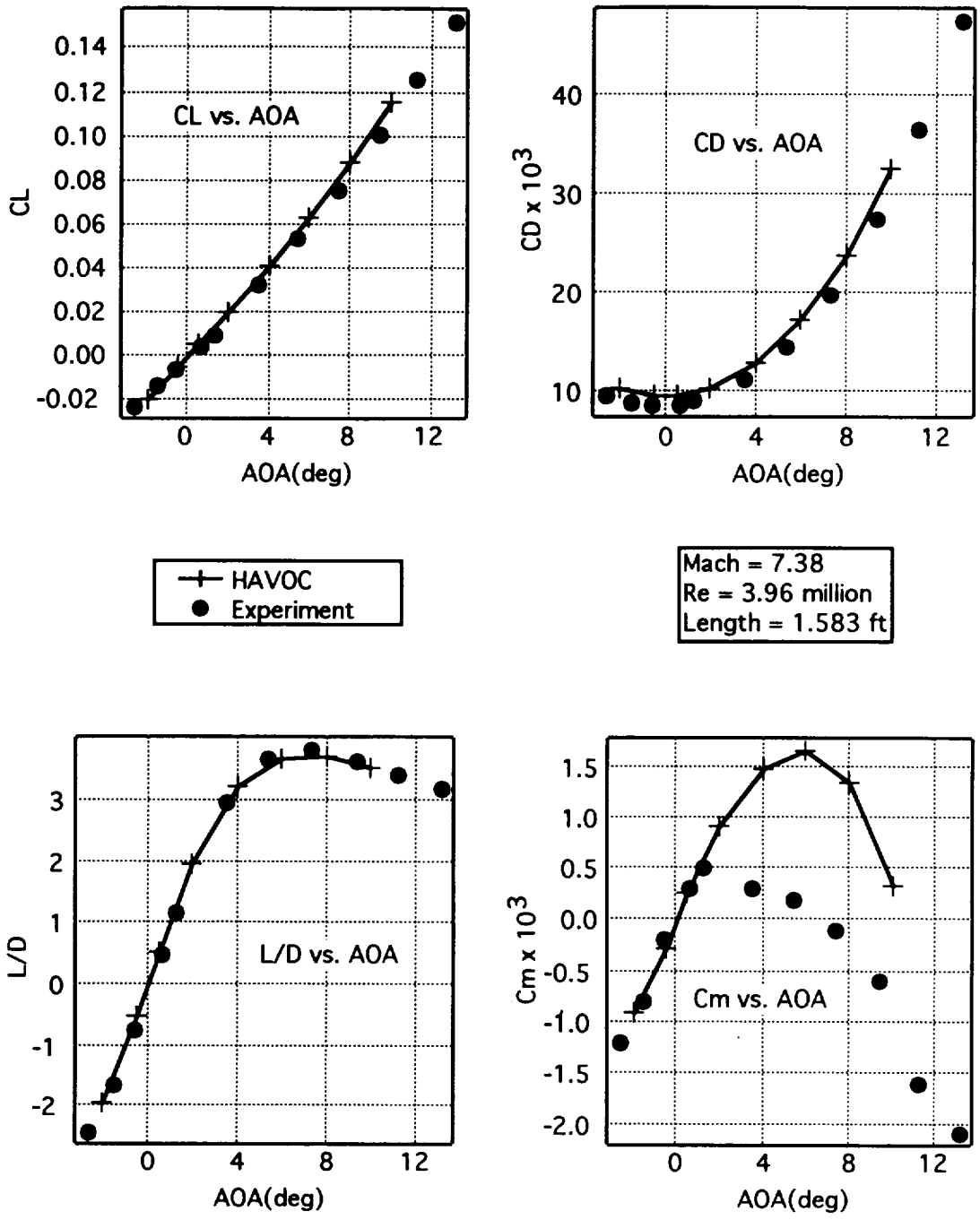

Figure 5.11. All-body Results, Mach 7.38, Tangent Wedge & Prandtl-Meyer Methods

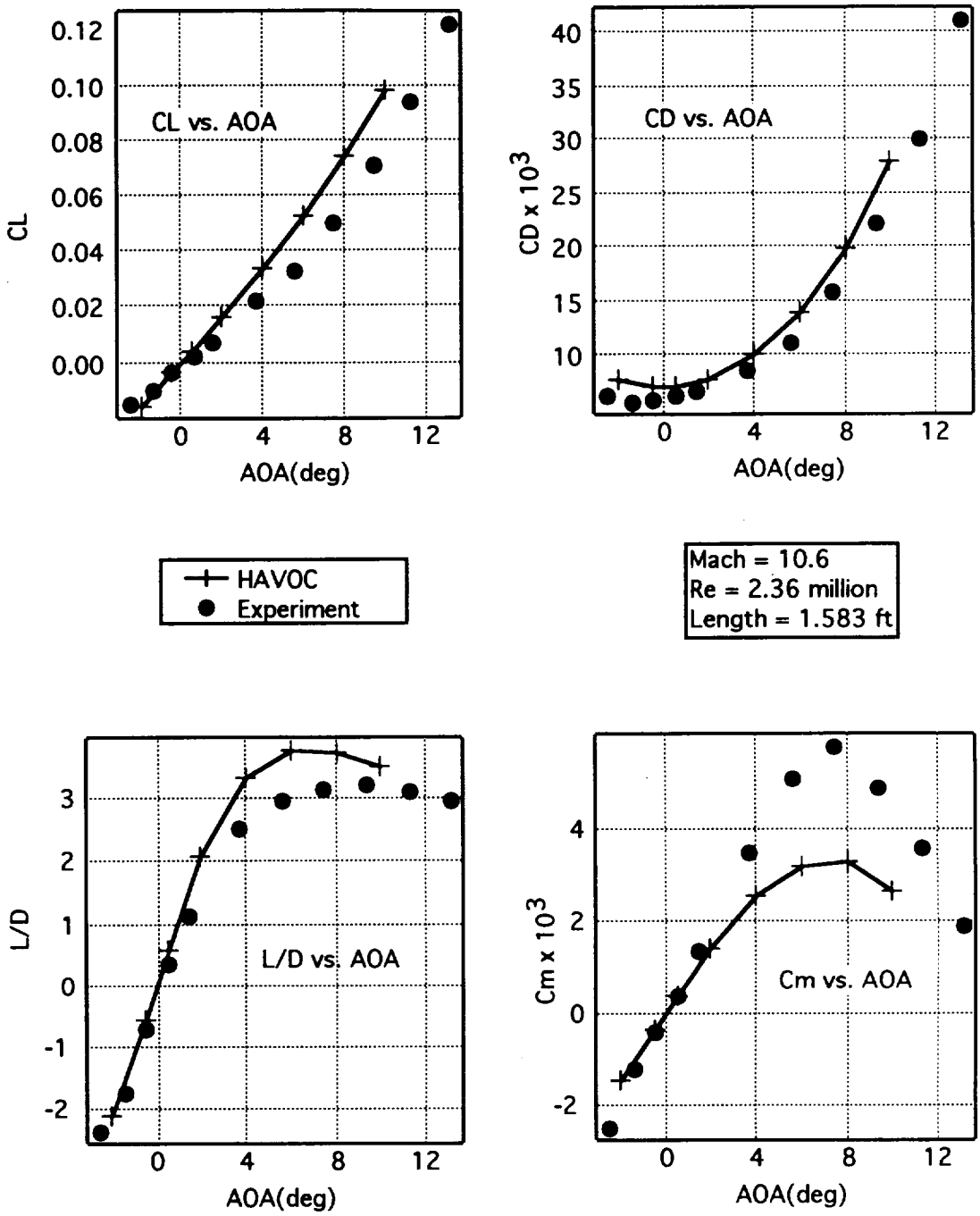

Figure 5.12. All-body Results, Mach 10.6, Tangent Wedge & Prandtl-Meyer Methods

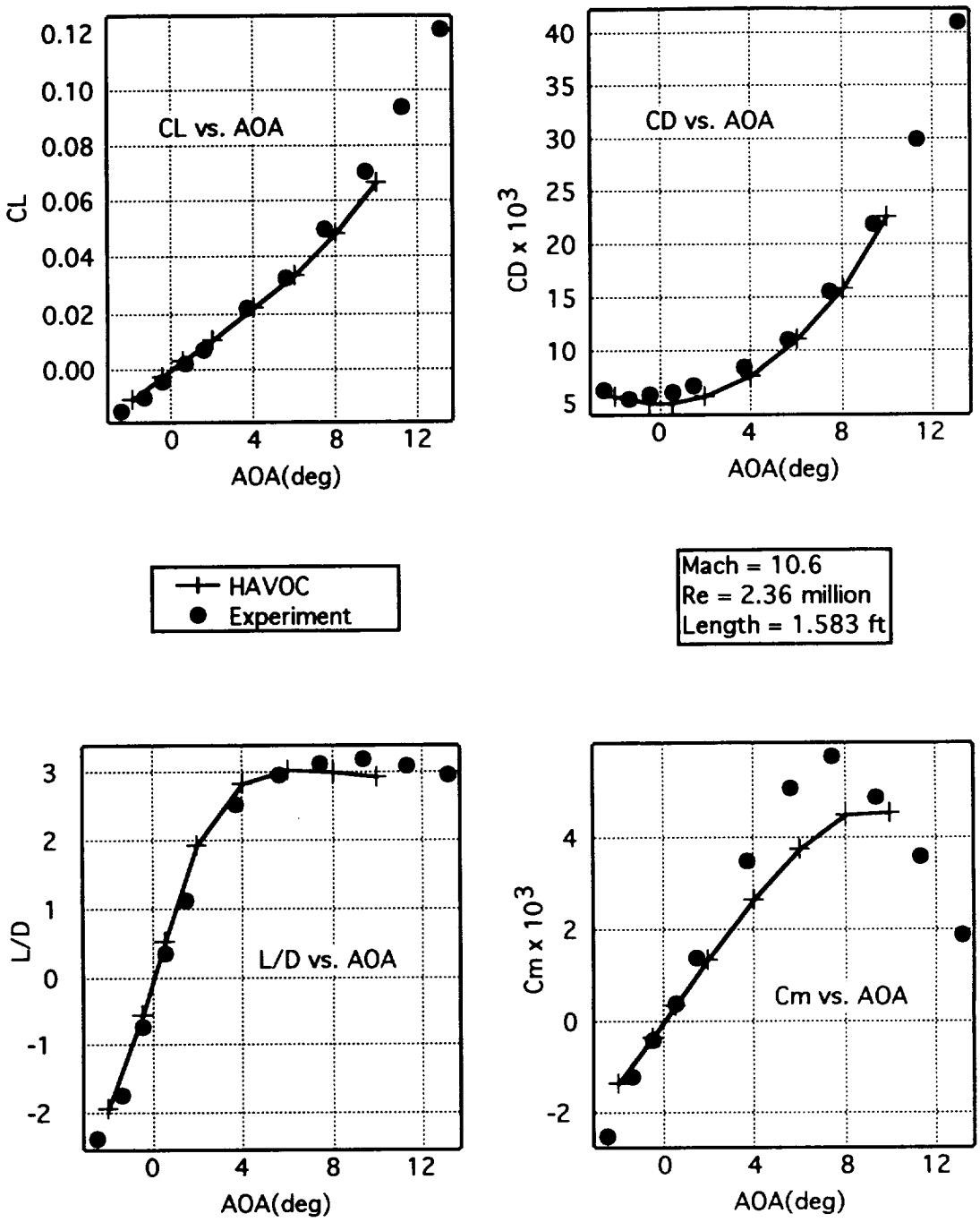

Figure 5.13. All-body Results, Mach 10.6, Newtonian Method

Mach 8 Waverider Analysis

Effect of Fairing and Engine on Waverider Performance

As mentioned in Chapter 3, a fairing has enormous effects on the waverider's performance, some of which are adverse. In this section, L/D ratios will be presented for a Mach 8 waverider in three different configurations: the pure waverider, the waverider with a fairing, and the waverider with a fairing and a scramjet engine. The three configurations are shown in Figure 5.14. All three were generated by the Waverider code.

The Waverider code is capable of propulsion analysis, but it is not used. The third configuration is the only one to include the engine. The panels representing the scramjet system (the ramps, inlet, combustor and nozzle) are not included in the aerodynamic analysis, since the Waverider code does not calculate pressure coefficient for that area. The engine cowl, which covers the engine from the inlet to the end of the combustor, is not shown in Figure 5.14. For the off-design analysis, in which only the HAVOC code is used, the whole geometry including panels in the engine area were included in the analysis. This represents the Waverider in power-off mode, in which the cowl of the scramjet engine conforms to the body shape. A configuration with an engine is included in order to make the waverider as close to a complete configuration as possible.

The geometry is altered at the base when imported into HAVOC. To model a vertical base, the last two stations must be on top of each other. HAVOC requires that each station be equally spaced, so the base becomes inclined, as shown in Figure 5.15. With enough stations, this problem can be minimized.

Figure 5.16 shows the effect of the fairing and the engine on the waverider's performance as analyzed by the Taylor - Maccoll Equations. The

L/D ratio for the vehicle with a lone fairing and the vehicle with a fairing and an engine is significantly lower than for the pure waverider. This is caused by the flow separation around the fairing, which creates low pressure and increases drag. The negative Cp's are noted in Figure 5.17, which shows Cp distribution over the bottom surface of the pure waverider and the waverider with the fairing. The light area over the fairing represents high negative pressures, which indicates separated flow, thereby reducing the L/D. If the initial turning angle of the fairing is reduced enough so that the flow wouldn't separate, some of the pressure would be recovered along the remaining fairing surface.

Since the on-design analysis excludes the engine area and the off-design analysis includes it, a comparison of the L/D ratios for the complete configuration and the configuration without the engine area is of value and is shown in Figure 5.18. The data indicate that including the engine does degrade the performance significantly, even though it is only a small percentage of the total vehicle area. For the configuration with the engine, drag is created on the ramps, and the flow separates over the nozzle, and creates more drag and loss of lift. Nevertheless, the total configuration with the engine is the more realistic, and will be used for the rest of the off-design analysis.

Note from Figure 5.18 that maximum L/D does not occur at the on-design condition. In this case it occurs at about 2° angle of attack. Maximum L/D = 4.5 for the total configuration and 5.2 for the configuration without the engine.

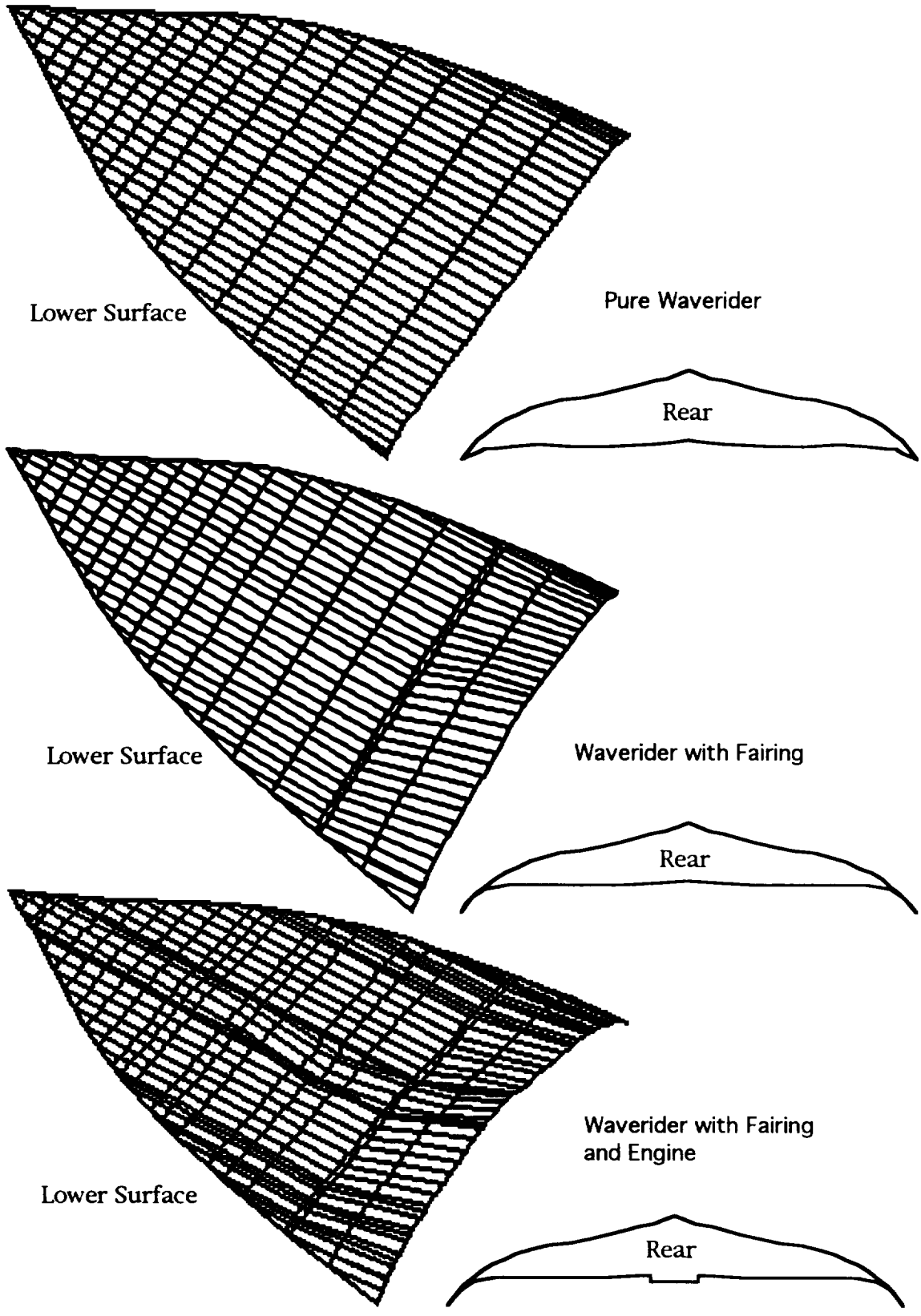

Figure 5.14. Three Mach 8 Waverider Configurations

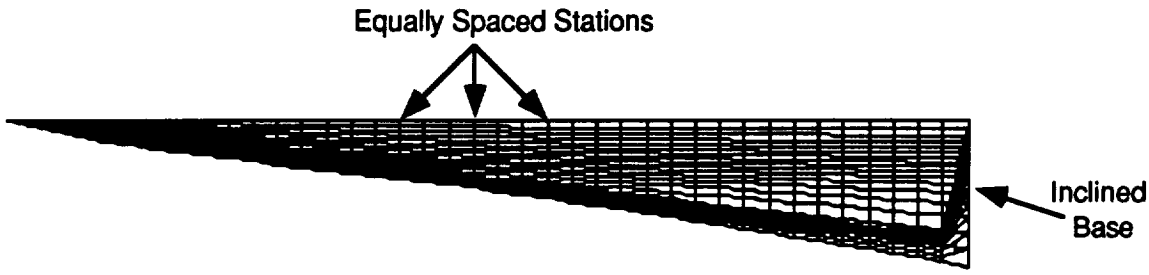

Figure 5.15. Pure Mach 8 Waverider Geometry in HAVOC Code

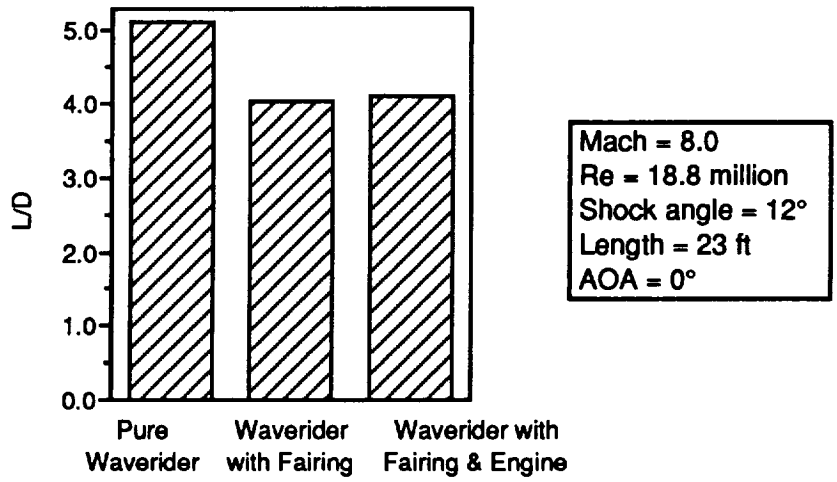

Figure 5.16. Taylor - Maccoll Results of Three Mach 8 Waverider Configurations

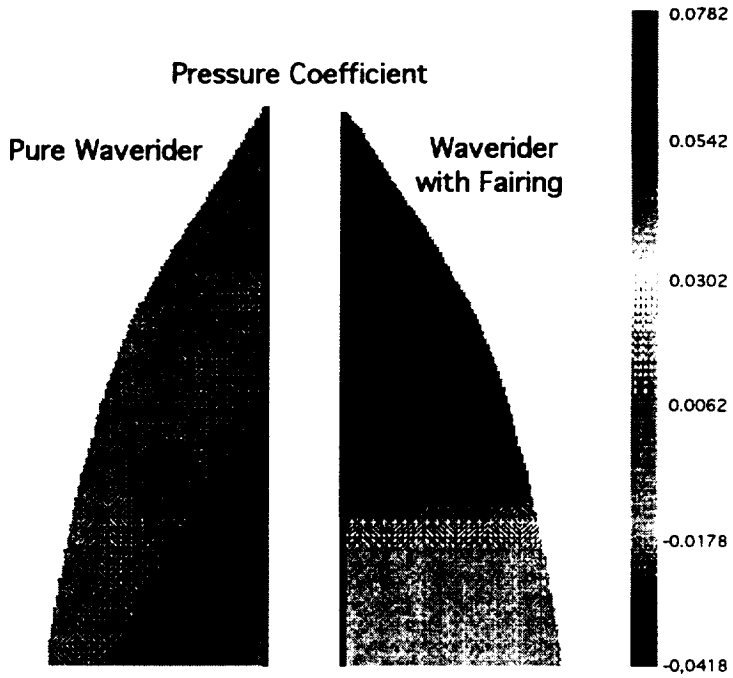

Figure 5.17. Pressure Distributions Over Lower Surfaces of Two Mach 8 Waverider Configurations

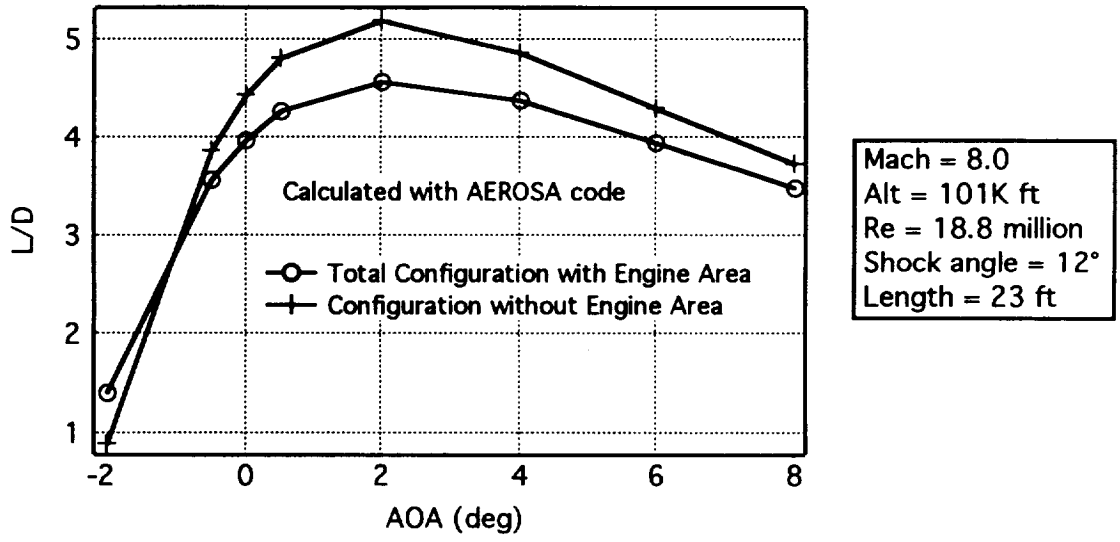

Figure 5.18. Effect of Engine on Mach 8 Waverider Performance

Comparison of Analysis Methods

Each of the three configurations in Figure 5.14 was analyzed by two methods; The Taylor - Maccoll Equations in the Waverider code and the Tangent Wedge / Prandtl - Meyer in HAVOC. The Tangent Wedge / Prandtl Meyer method will hereafter be called the Tangent Wedge method for simplicity.

Figure 5.19 shows the L/D values from both methods for each configuration. Agreement between the two methods is excellent. For the pure waverider configuration, the Taylor - Maccoll method produced an L/D = 5.16. Since only this method accounts for the beneficial waverider effects (the other method is an independent panel method), it should have slightly higher pressure on the lower surface and better L/D values. There is only a small difference between the two values of 0.75%.

For both cases with the fairing, the Taylor - Maccoll solution has lower L/D ratios than the Tangent Wedge method. This is a result of the individualized panel method not accounting well for separated flow. The first station of panels on the fairing may be inclined aft at a very high incidence and the pressures will be minimum, but farther back the panels will be inclined less aft and the pressures will increase. Since the Taylor - Maccoll solution keeps track of panels coordinates relative to each other, it can account for separation. Once the flow becomes separated at a panel, it must stay separated on the surface behind it. The individualized panel method does not account for separation on other panels, and therefore gives an optimistic L/D ratio for any vehicle with a fairing.

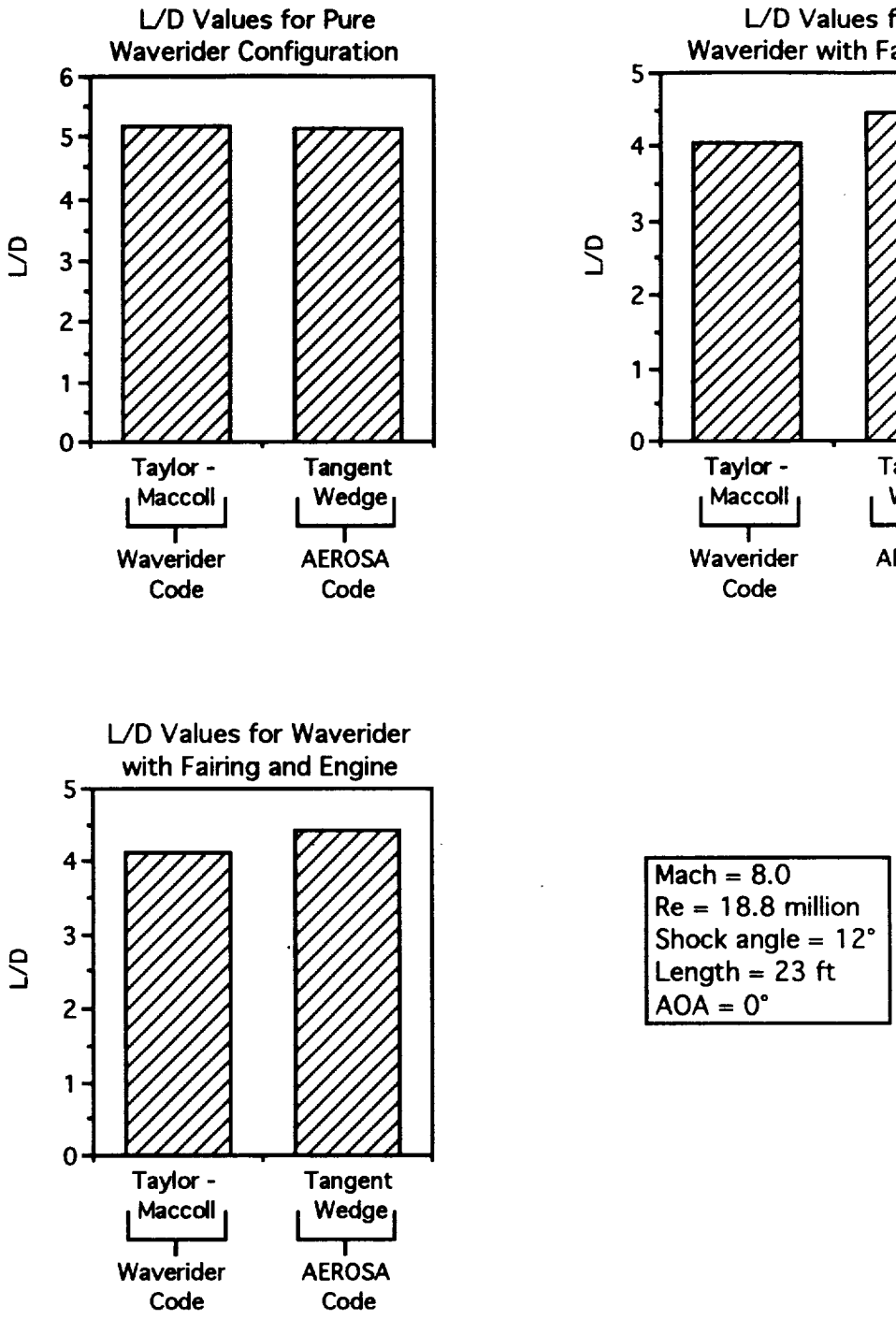

Figure 5.19. Effect of Fairing on Mach 8 Waverider Performance

Pitching Moment and Force Coefficient Results

The waverider is only on-design at a single angle of attack and Mach number. At any other condition, the flow will not be conical and the shock wave will not be attached to the leading edge. This next section considers how the waverider performs at off-design conditions. Since the Taylor - Maccoll equations are not valid for off-design conditions, HAVOC was used. The Tangent Wedge method is used for all impact panels and the Prandtl - Meyer method is used for all shadow panels.

Both the Mach 8 and the Mach 14 waveriders used for the stability analysis included a fairing. The effect of a fairing on Cm can be explained as follows: Hypersonic vehicles generally tend to have very high forebody pressures, creating a pitch up tendency. The fairing creates negative pressures at the rear of the vehicle's lower surface. This causes a downward force at the rear of the vehicle and an even larger nose up pitching moment.

To assist in the stability analysis, an elevator module was added to the AEROSA code (see Appendix). The elevator module was not added to HAVOC. The elevator module simulates elevators at the trailing edge of the waverider. Inputs are given describing the size and placement of the elevator. The module does not change the shape of the vehicle body. Instead it changes the normal components and angle of deflection of each panel within the elevator area (see Figure 5.20). This is possible in an independent panel method such as AEROSA, and since the panel's normal component is all that is used to determine Cp, the module works just as well as if the body shape were actually changed.

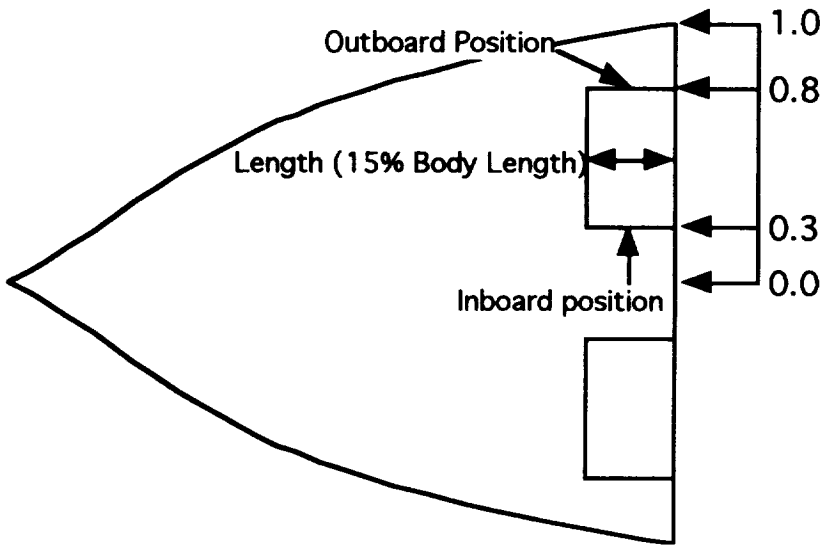

Figure 5.20. Mach 8 Waverider with Elevators

Figure 5.21 shows pitching moment charts for three different Center of Gravity (CG) locations, ranging from 45% to 55% body length. Each chart shows four curves, each at different elevator deflections. The elevator dimensions used for this configuration are shown in Figure 5.20. The ideal waverider exhibits the following characteristics: 1) longitudinal static stability, or negative slope of the Cm vs. AOA curve; 2) zero Cm value at zero AOA (trim condition), which is necessary for cruise (AOA must be zero for the waverider characteristics to exist), and 3) minimum elevator deflection to achieve trim. Characteristic 2 is the only one that is absolutely required. Trim conditions must exist for cruise. If the waverider is unstable, an artificially stable active control system can be used. Elevator deflection can also be tolerated for trim, but it may affect lift and drag.

This Mach 8 Waverider is longitudinally statically stable at CG = .45L and .50L (L is body length of the waverider), but is unstable at CG = .55L. It is desirable to locate the CG as far forward as possible in order to make the vehicle stable. At CG = .55L, the trim requirement cannot be met without

elevator deflection larger than 12°. The trim point for CG = .50L occurs at an elevator deflection of 10°. This case meets all three requirements listed above, but requires a C.G. location that is hard to achieve.

Figure 5.22 shows the effect of elevator deflection on the lift, drag, and L/D curves for the Mach 8 waverider (The L/D curve for zero degrees deflection is the same as the curve in Figure 5.19). There is a small increase in lift as the elevator is deflected, but the change in drag is negligible. The Cm values are significantly more affected because the elevator is located at the rear of the vehicle, and has a long moment arm. The L/D ratios increase slightly with increased elevator deflection, due to the small increase in lift.

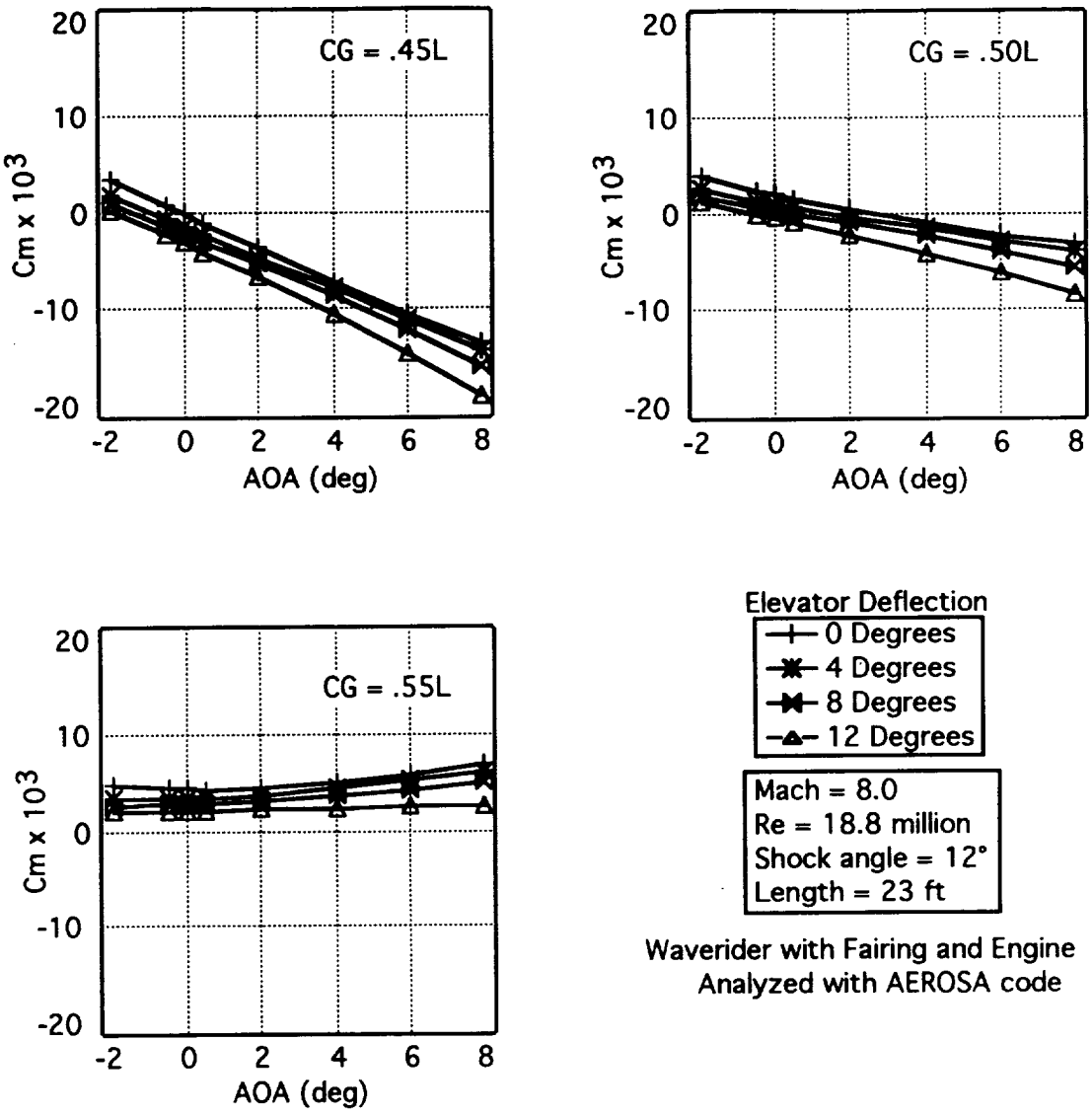

Figure 5.21. Mach 8 Waverider Pitching Moment Characteristics

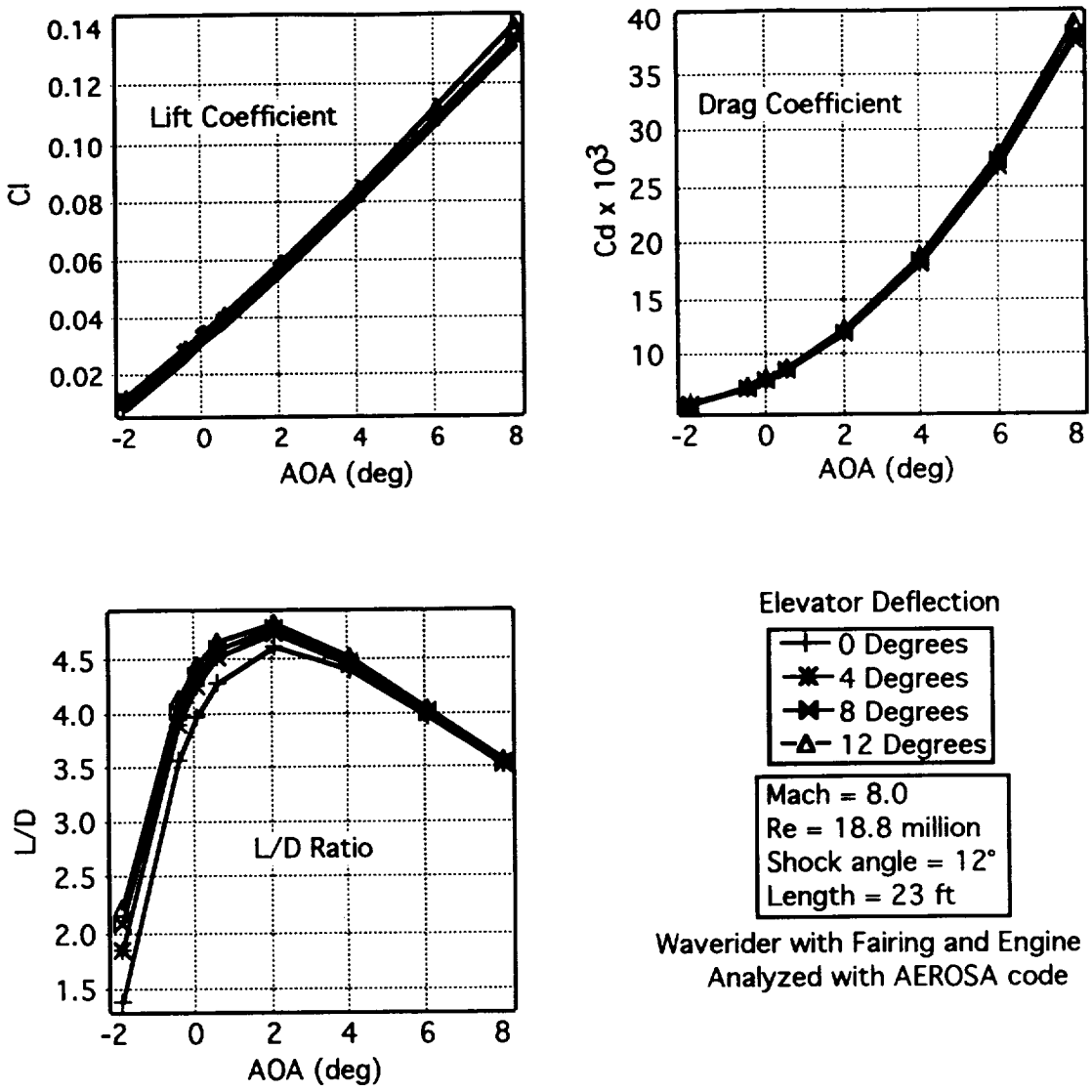

Figure 5.22. Mach 8 Force Coefficients

Mach 14 Waverider Analysis

The second waverider to be presented is designed to fly at Mach 14. At higher Mach numbers, the conical shock is closer to the generating cone. These waverider shapes are generally more slender than those at low Mach numbers.

At speeds above Mach 10, real gas effects must be considered. The Wavrider code uses a real gas model that follows that of Gordon and McBride [Ref. 15]. The Waverider code gives the option of using a real gas model or an ideal gas model for the flow analysis. The code with the ideal gas model runs slightly faster than one with the real gas model, and is used for speeds below Mach 10. Since this Waverider is designed for Mach 14, the real gas model is used.

Figure 5.23 shows the Mach 14 waverider including the fairing and the engine system. The generating curve (which looks like the back view of the freestream surface) is just a straight line, whereas the Mach 8 waverider's generating curve is curved. At higher Mach numbers, this type of body shape tends to give the best performance.

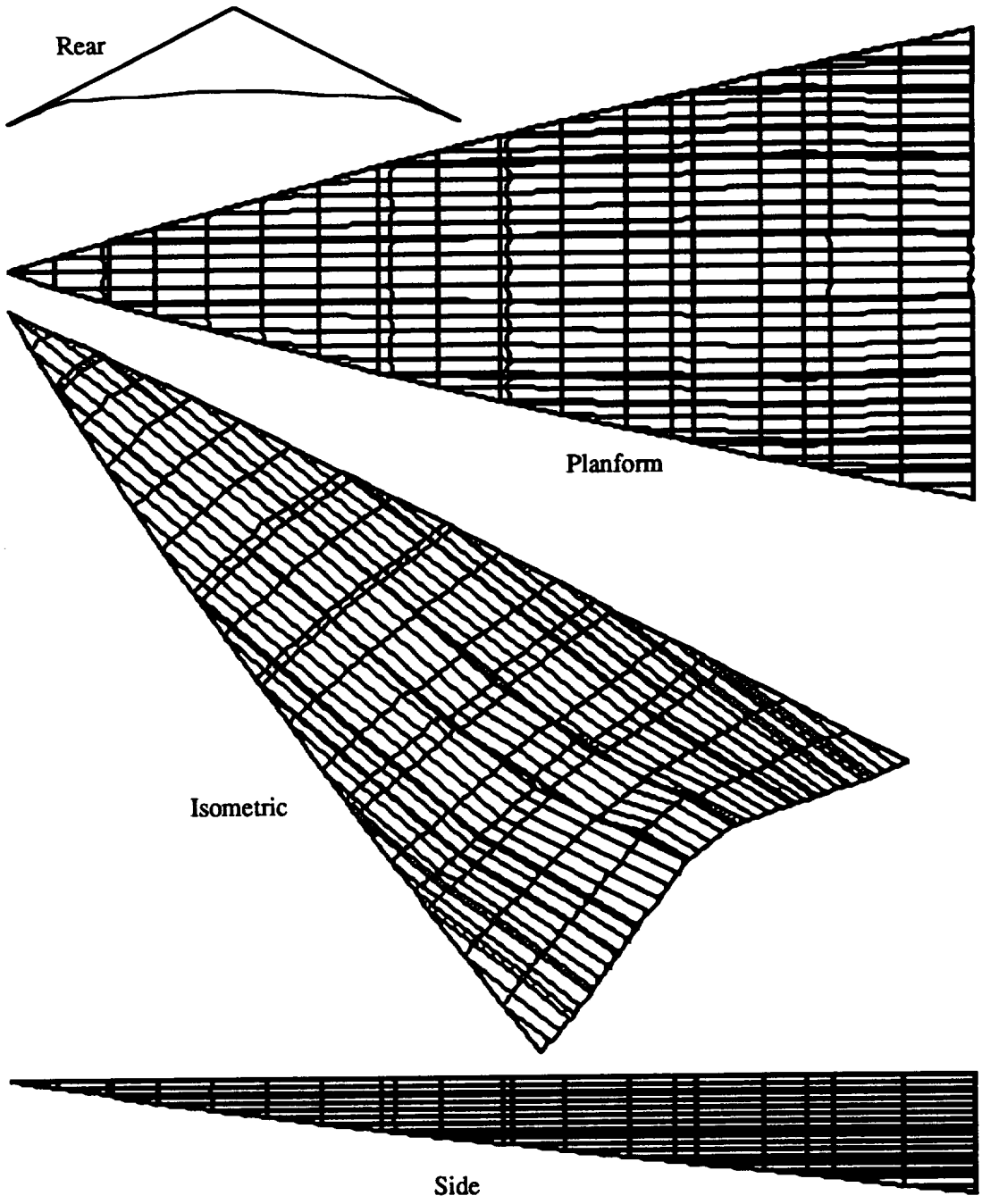

Figure 5.23. Mach 14 Waverider

Comparison of Analysis Methods

At Mach 14, the Newtonian method, which was validated for high Mach numbers, is also used for analysis along with the Taylor - Maccoll and the Tangent Wedge / Prandtl - Meyer methods. The Taylor - Maccoll solution is considered the most accurate method of the three, since it uses the fewest and the most reasonable assumptions. Figure 5.24 shows the on-design results for all three methods for the Mach 14 Waverider. The Newtonian method predicts values of both CL and CD that are significantly lower than those predicted by the Taylor - Maccoll solution. The Tangent Wedge solution (which includes Prandtl - Meyer for the shadow region) compared favorably with the Taylor - Maccoll solution, and will be used in AEROSA for the stability analysis.

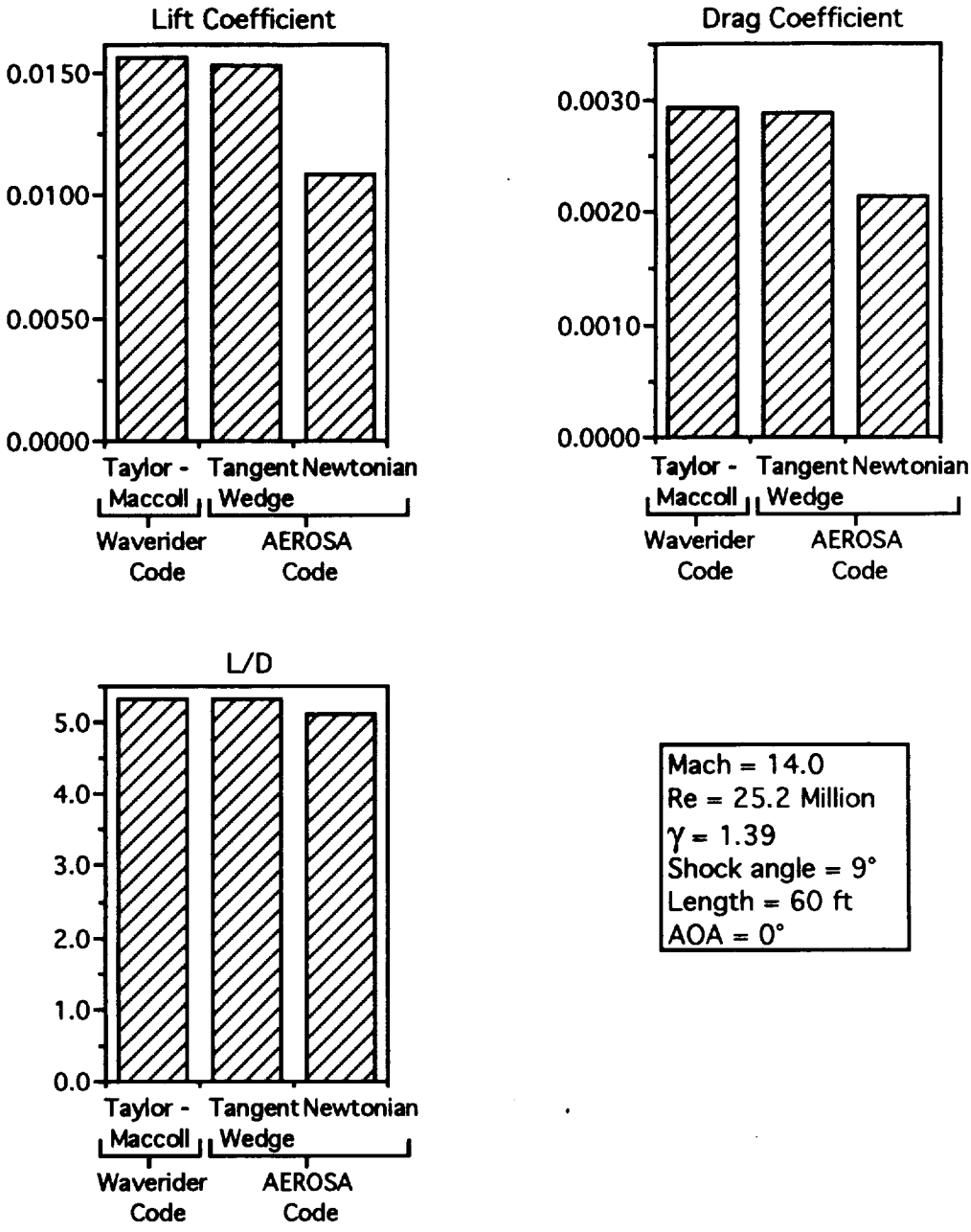

Figure 5.24. On-design Results for Mach 14 Waverider

Pitching Moment and Force Coefficient Results

Figure 5.25 shows the pitching moment characteristics for the Mach 14 waverider at 3 different CG locations. The data indicates that the static stability and trim conditions are more easily met for the slender Mach 14 design. Both

conditions can be met with 4° elevator deflection for a CG at 50% body length, or with 9° elevator deflection for a CG at 55% body length. Locating the CG at 55% body length is reasonable. For the Mach 8 waverider to remain stable, the farthest aft position of the CG is 50% body length. For the Mach 14 waverider, trim can be met at 60% CG with about 13° elevator deflection, and the vehicle is slightly unstable.

At Mach 14, the elevators have more effect on the lift and drag characteristics than they did at Mach 8. Figure 5.26 shows the force coefficients and the L/D ratio for the Mach 14 Waverider. 12° deflection increases both CL and CD by about 20%. L/D max occurs at about 1° AOA, which is lower than that for the Mach 8 waverider.

Figure 5.25 shows that as the C.G. moves farther aft, more elevator deflection is required to achieve trim. Figure 5.26 shows that drag increases with increased elevator deflection. Therefore, aft C.G. location results in increased drag. This shows that achieving a C.G. as far forward as possible is beneficial for aerodynamic reasons as well as stability reasons.

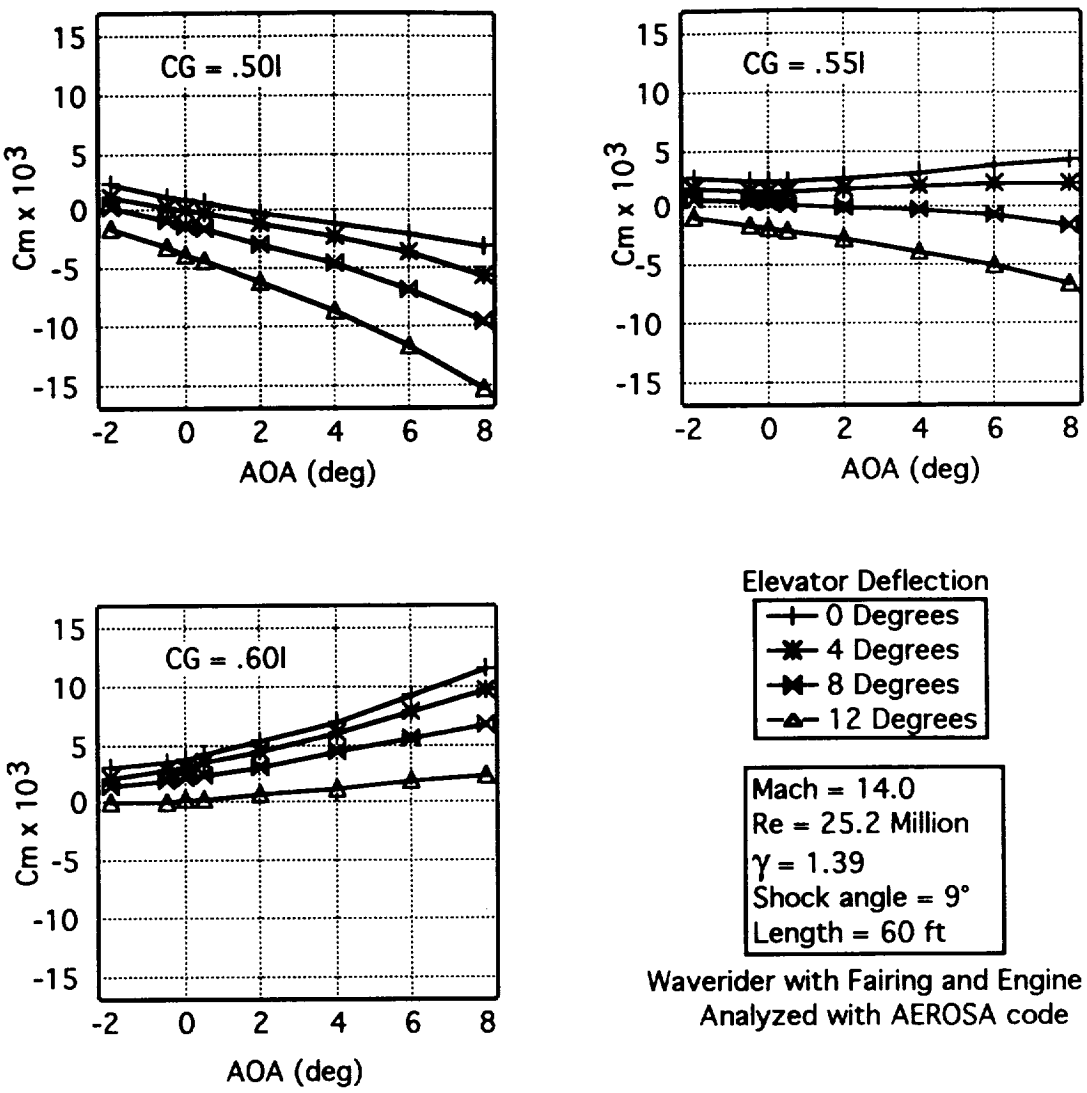

Figure 5.25. Mach 14 Waverider Pitching Moment Characteristics

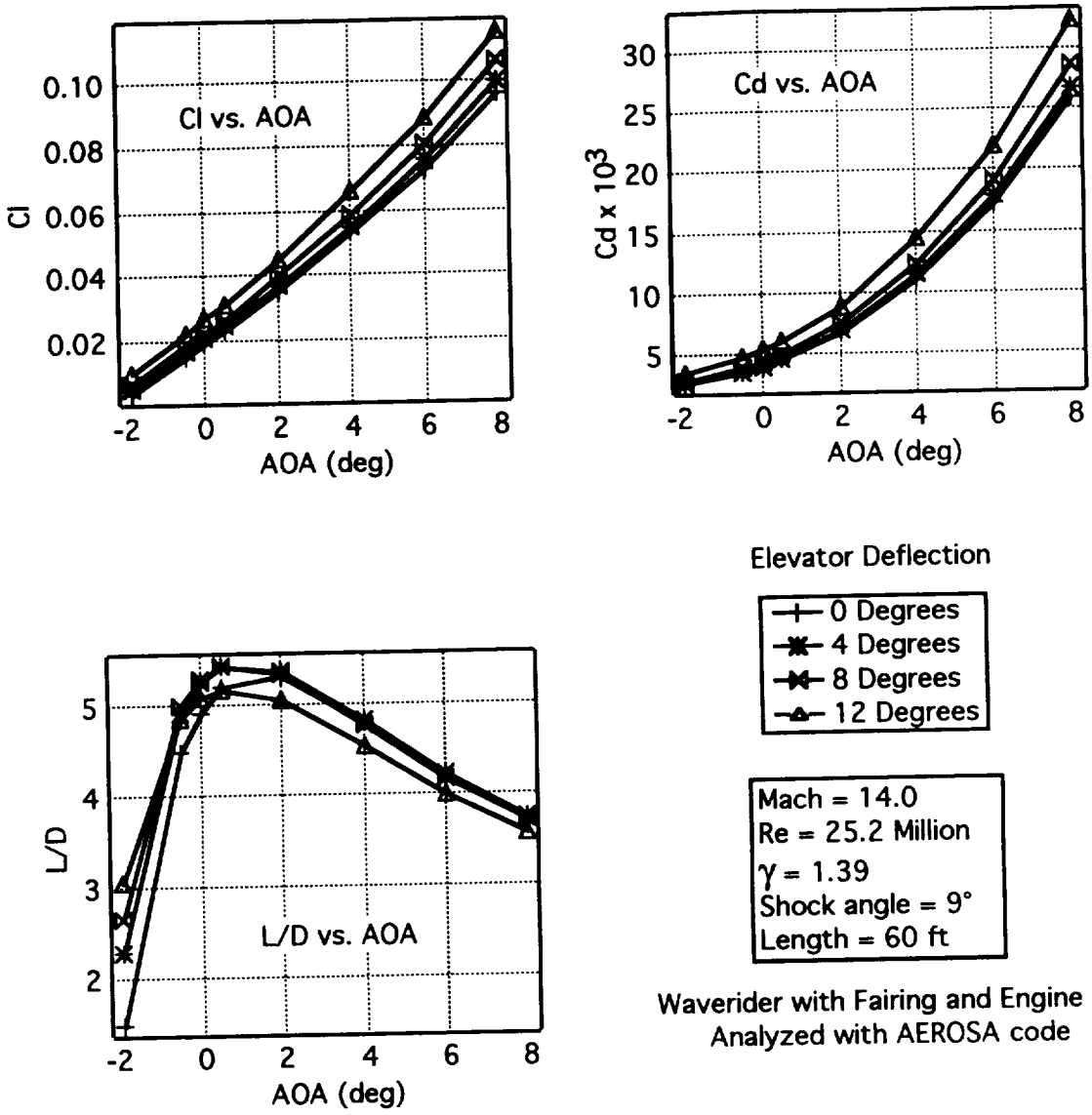

Figure 5.26. Mach 14 Force Coefficients

CHAPTER 6

Conclusions

In this report, two computer codes have been validated using either experimental data or published results. The Waverider code, which employs the Taylor - Maccoll Equation for conical flow, was shown to compare well with results published by Rasmussen and He. HAVOC (and AEROSA), a code which uses various approximate techniques for hypersonic vehicle analysis, was shown to be well suited for conceptual vehicle design through a comparison with experimental results on a hypersonic all-body test model.

In an attempt to make the waverider closer to a realistic configuration, the Waverider code was modified to generate a fairing. The fairing permits more pressure recovery and reduction of drag than for vehicles with a bluff base. AEROSA was modified to include elevators on the waverider. Elevator deflections were necessary to achieve trim for most waveriders considered. The two codes were then used to generate and analyze a Mach 8 and a Mach 14 Waverider. The fairing deteriorated the performance of both waveriders. The Mach 8 Waverider had an L/D = 5.2 without the fairing, and an L/D = 4.4 with the fairing. Nevertheless, the fairing is still necessary, because a bluff based waverider will not be adequate for a vehicle that must fly through a full velocity range.

Both waveriders include shapes for scramjet engine systems for their stability analysis. Although the vehicle shapes with engines degraded in

aerodynamic performance, engines are a necessary part of the total vehicle configuration.

Cm values of various configurations about several CG locations were computed with and without elevator deflection. For the Mach 8 configuration, the CG must be at 50% of the body length for the vehicle to be stable and to achieve trim with 10° elevator deflection. If the CG is farther aft, then the vehicle becomes unstable and trim becomes impossible to reach without large elevator deflections. Achieving a CG farther forward than 50% is very difficult.

At Mach 14, real gas effects were accounted for. The on-design L/D of 5.2 is much higher than the on-design L/D for the Mach 8 waverider. Also, the Mach 14 waverider was more stable, achieving statically stable trim at a CG = 55% body length and an elevator deflection of 9°.

Possibilities for further work in the area of waverider aerodynamics include:

(1) Studying the effects of a fairing on the upper surface instead of on the lower surface. The lower surface would not have low pressure due to expansion of the flow, which creates a downward force. The upper surface would have flow expansion which would create extra drag, just as it does on the lower surface, but the low pressure on the upper surface would add to the upward lift force. A waverider with an upper surface fairing would have better L/D values and lower Cm values than a comparable waverider with a lower surface fairing.

(2) Studying aerodynamic and stability characteristics at off - design Mach numbers. Since HAVOC (and AEROSA) has been modified, this area can easily be looked into. It is also necessary to study these characteristics at subsonic and transonic speeds, requiring a different analysis tool, since HAVOC is not valid at low speeds.

(3) Optimization of waveriders with fairings. Optimization tools are available and have been used with the Waverider code, but not for waveriders with fairings. The Mach 8 waverider presented in this study was optimized before it included a fairing. The fairing was incorporated afterwards. One question to be answered is how much a fairing would change the overall optimized waverider body shape.

References

1. Nonweiler, T. R. F., "Delta Wings of Shape Amenable to Exact Shock Wave Theory," J. Royal Aero. Soc., Vol. 67, 1963, p. 39.

2. Beuerlein, David L., "Optimization of Waveriders to Maximize Mission Performance," General Dynamics, Fort Worth Division, 1990.

3. Bowcutt, Kevin G., Anderson, John D. Jr., and Capriotti, Diego, "Viscous Optimized Hypersonic Waveriders," Department of Aerospace Engineering, University of Maryland, 1987.

4. O'Neill, M. K., and Lewis, M. J., "Optimized Scramjet Integration on a Waverider," University of Maryland, 1991.

5. Anderson, John D. Jr., Modern Compressible Flow with Historical Perspective, McGraw-Hill Book Company, New York, 1990.

6. Gregory, Thomas J., Ardema, Mark D., Water, Mark H., "Hypersonic Transport Preliminary Performance Estimates For an All-Body Configuration," AIAA Paper 70-1224, 1970.

7. Rasmussen, Maurice L., He, Xiaohai, "Analysis of Cone-Derived Waveriders by Hypersonic Small-Disturbance Theory," University of Oklahoma, 1991.

8. Taylor, G. I., and Maccoll, J. W. , "The Air Pressure on a Cone Moving at High Speed," *Proc. Toy. Soc.* (London) ser. A, vol. 139, 1933, pp. 278-311.

9. Anderson, John D. Jr., Hypersonic and High Temperature Gas Dynamics, McGraw-Hill Book Company, New York, 1989.

10. Shapiro, Ascher H., The Dynamics and Thermodynamics of Compressible Fluid Flow, The Ronald Press Company, New York, 1954.

11. Bertin, John J., and Smith, Michael L., Aerodynamics for Engineers, Prenice-Hall, Inc., Englewood Cliffs, N.J., 1979.

12. Ames Aeronautical Laboratory, Moffet Field, CA, Equations, Tables, and Charts For Compressible Flow, NACA Report 1135, 1953.

13. Newton, Isaac, *Principia*, Propositions 34 and 35, 1687.

14. Nelms, Walter P., and Thomas, Charles L., "Aerodynamic Characteristics of An All-Body Hypersonic Aircraft Configuration at Mach Numbers From 0.65 to 10.6," NASA Report TN D-6577, 1971.

15. Gordon, Sanford, and McBride, Bonnie J., "Computer Program for Calculation of Complex Chemical Equilibrium Composition, Rocket Performance, Incident and Reflected Shocks, and Chapman - Jouguet Detonations," NASA Special Publication SP-273, 1971.

Appendix

Original Computer Code Listings

Fairing Generation and Modification Routines for Waverider Code

Section of Subroutine WAVRDR

Subroutine WAVRDR (that is spelled correctly) is the main portion of the Waverider code. This next section and the following two subroutines were added to subroutine WAVRDR.

```
C---*----1----*----2----*----3----*----4----*----5----*----6----*----7--
C Generate Fairing for rear of waverider.  XCLOSE is the base thickness
C as a % of fairing length.  After phi = .8phimax, the fairing becomes
C linear, and the base thickness linearly decreases to zero.  If the
C leading edge is past zrear then zrear becomes leading edge.The initial
C angle of the parabolic fairing decreases linearly as phi increases.
C RL and OMEGL are the resulting changed coordinates. If ZFAIR2 > .99,
C then the whole section is skipped, and no fairing is made.
C Arclength, SL, is recalculated.
C


      ZFAIR = (ZFAIR2) * (1.0 - ZNOSE) + ZNOSE
      IF (ZFAIR2 .LE. .99) THEN
         DEND = XCLOSE * (1 - ZFAIR)
         DELEND = DEND
         PHIMAX = APHI(NPHI)
```

```
      CLSPT = .9

      DO 650 IPHI = IPHIE, NPHI

         ZRFLAG = .FALSE.
         LIN = LINEAR
         IF ( APHI(IPHI) .GT. CLSPT*PHIMAX ) THEN
            LIN = .TRUE.
            DELEND = DEND*(1./(1.-CLSPT))*(PHIMAX-APHI(IPHI))/
     1                PHIMAX + .0001
         ENDIF
         Z1 = RL(1,IPHI) * COS ( OMEGL(1,IPHI) )
         IF (Z1 .GT. ZFAIR) ZFAIR = Z1

         ZENDF = RU(NI(IPHI),IPHI) * COS ( OMEGU(NI(IPHI),IPHI) )
         XENDF = RU(NI(IPHI),IPHI) * SIN ( OMEGU(NI(IPHI),IPHI) )
         XENDF = XENDF + DELEND

         DO 750 IZ = 1,NI(IPHI)

            Z = RL(IZ,IPHI) * COS ( OMEGL(IZ,IPHI) )

            IF( Z .GT. ZFAIR+.00001 .AND. .NOT. ZRFLAG ) THEN
               AIZF(IPHI) = IZ-1
               APF(IPHI) = AP(IZ-1)
               ATF(IPHI) = AT(IZ-1)

               IF (IZ .GT. 1) THEN
                  XOLD = RL(IZ-1,IPHI)*SIN(OMEGL(IZ-1,IPHI))
                  ZOLD = RL(IZ-1,IPHI)*COS(OMEGL(IZ-1,IPHI))
                  X2 = RL(IZ,IPHI)*SIN(OMEGL(IZ,IPHI))
                  XFAIR = XOLD+(X2-XOLD)*(ZFAIR-ZOLD)/(Z-ZOLD)
               ELSE
                  XFAIR = RL(IZ,IPHI)*SIN(OMEGL(IZ,IPHI))
               ENDIF
```

```
                  IF  (IZ .GT.2) THEN
                     RL(IZ-1,IPHI) = SQRT(XFAIR*XFAIR + ZFAIR*ZFAIR)
                     OMEGL(IZ-1,IPHI) = ACOS( ZFAIR/RL(IZ-1,IPHI) )
                  ENDIF
                  ZRFLAG = .TRUE.
               ENDIF

               IF ( ZRFLAG ) THEN
                 PERCPHI = APHI(IPHI) / PHIMAX
                  CALL PARABOLA(Z,ZFAIR,XFAIR,ZENDF,
     >                          XENDF,INITANG,PERCPHI,LIN,X)

                  XUP = RU(IZ,IPHI)*SIN(OMEGU(IZ,IPHI))+.0001
                  IF (X .LT. XUP) X = XUP

                  DS = SQRT( (X-XOLD)**2 + (Z-ZOLD)**2 )
                  SL(IZ,IPHI) = SL(IZ-1,IPHI) + DS
                  RL(IZ,IPHI) = SQRT(X*X + Z*Z)
                  OMEGL(IZ,IPHI) = ACOS( Z/RL(IZ,IPHI) )
                  XOLD = X
                  ZOLD = Z
               ENDIF
  750       ENDDO
  650    ENDDO

C---*----1----*----2----*----3----*----4----*----5----*----6----*----7--

C
C REBUILD ARC LENGTH, PRESSURE AND REYNOLDS NUMBER TABLES
C
         CALL FAIRANAL(RL,OMEGL,IPHIE,NPHI,AIZF,APF,ATF,NI,REPFT,M1,
     1                 TINF,PINF,RHOINF,GAMA,ACP,ARHORT,AAMACH,AREPFL,
     2                 QRAT,CPMIN)

      ENDIF
```

Subroutine PARABOLA

Subroutine PARABOLA is the code that actually generates the parabolic curve. It is called from the WAVRDR subroutine(above).

```
C********1*********2*********3*********4*********5*********6*********7**
      SUBROUTINE PARABOLA (X,X1,Y1,X2,Y2,INITANG,PERCPHI,LINEAR,Y)
C
C ACRONYM
C     PARABOLA
C     ********
C
C PURPOSE
C     Given the nozzle start point(X1,Y1), the nozzle end point (X2,Y2),
C     the nozzle turn angle (THETA), and the X location(X), find the
C     Y location on the nozzle.  The nozzle is modeled by the following
C     parabolic equation:
C
C        YN = A + B*X + C*X^2
C
C     where
C
C        DENOMINATOR = X1^2 - 2*X1*X2 + X2^2
C        C = [ TAN(THETA)*(X1-X2) - (Y1,Y2) ] / DENOMINATOR
C        B = TAN(THETA) - 2*C2*X1
C        A = Y1 - C1*X1 - C2*X1^2
C
C ARGUMENTS
C     TYPE         VARIABLE       I/O  DESCRIPTION
C.....................................................................
C
      REAL         X          !  I   X location on nozzle
      REAL         X1         !  I   X start of nozzle
      REAL         Y1         !  I   Y start of nozzle
      REAL         X2         !  I   X end of nozzle
      REAL         Y2         !  I   Y end of nozzle
```

```
      REAL          PERCPHI     !  I   PERCentage of PHI
      REAL          INITANG     !  I   INITial nozzle ANGle
      LOGICAL       LINEAR      !  I   use LINEAR nozzle if true
      REAL          Y           !  O   Y location on nozzle
C
C SUBROUTINES
C     NAME          DESCRIPTION
C-----------------------------------------------------------------
C     none.
C
C ENVIRONMENT
C     Machine:                  IRIS 4D
C     Operating System:         UNIX
C     Language:                 FORTRAN 77
C
C AUTHOR
C     David pessin
C     Cal Poly, SLO
C
C CHANGE HISTORY
C     DATE          DESCRIPTION
C-----------------------------------------------------------------
C     Sept 92  dnp  Original release - MOD 0.
C
C-*******1*********2*********3*********4*********5*********6*********7**
C
C COMMON PARAMETER VALUES
C     TYPE          VARIABLE              DESCRIPTION
C-----------------------------------------------------------------
C     none.
C
C LOCAL DECLARATIONS
C     TYPE          VARIABLE        VAL   DESCRIPTION
C-----------------------------------------------------------------
C
      REAL          A,B,C       !  coefficients of parabolic eqn.
```

```
      REAL          TTHETA      !  TANgent of INITANG
      REAL          DEGRAD
      PARAMETER    (DEGRAD = 0.01745329252)
C
C
C
C=====================================================================
C

      TTHETA = TAN( -INITANG * DEGRAD ) * (1.-PERCPHI)

      IF ( LINEAR ) THEN
         B = ( Y2 - Y1 ) / ( X2 - X1 )
         A = Y1 - B*X1
         Y = A + B*X
      ELSE
         DENOMINATOR = ( X1*X1 - 2*X1*X2 + X2*X2 )
         C = ( TTHETA*( X1-X2 ) + ( Y2-Y1 ) ) / DENOMINATOR
         B = TTHETA - 2*C*X1
         A = Y1 - B*X1 - C*X1*X1
         Y = A + B*X + C*X*X
      ENDIF

c      WRITE(55,30) X1,X2,ZREAR, THETA
  30  FORMAT (5(1X,F9.6))



C=====================================================================

      RETURN
      END

C********1*********2*********3*********4*********5*********6*********7*
```

Subroutine FAIRANAL

Subroutine FAIRANAL analyzes each panel in the fairing region. Since conical flow is no longer present, the surface pressures must be calculated using an approximate method. The Prandtl - Meyer expansion method is used for this analysis.

```
C********1*********2*********3*********4*********5*********6*********7**
      SUBROUTINE FAIRANAL(RL,OMEGL,IPHIE,NPHI,AIZF,APF,ATF,NI,REPFT,
     1                    MINF,TINF,PINF,RHOINF,GAMA,ACP,ARHORT,AAMACH,
     2                    AREPFL,QRAT,CPMIN)
C
C ACRONYM
C     AFT facing ramp ANALysis
C     ***              ****
C
C PURPOSE
C
C     Calculate the cp, prat, trat, mach number at each point for the
C     fairing of the lower surface of the waverider.  Then refill
C     cp, rho ratio, mach, repfl, and Q ratio Arrays.
C
C
C ARGUMENTS
C     TYPE          VARIABLE        I/O  DESCRIPTION
C.....................................................................
C
      REAL          RL(101,*)        !  I   R Lower
      REAL          OMEGL(101,*)     !  I   OMEGa Lower
      INTEGER       IPHIE            !  I   IPHI End of ramp
      INTEGER       NPHI             !  I   Number of PHI's
      INTEGER       AIZF(*)          !  I   Array IZ wher fairing strts
      REAL          APF(*)           !  I   Array Pres. whr frng strts
      REAL          ATF(*)           !  I   Array Temp. whr frng strts
      INTEGER       NI(*)            !  I   max Number of IZ
```

```
      REAL          REPFT              !  I   REynold's number Per FooT
      REAL          MINF               !  I   freestream Mach number
      REAL          TINF               !  I   Temperature INFinity
      REAL          PINF               !  I   Pressure INFinity
      REAL          GAMA               !  I   ratio of specific heats
      REAL          ACP(101,*)         !  O   CP ARray
      REAL          ARHORT(101,*)      !  0   Array RHO RaTio
      REAL          AAMACH(101,*)      ! I/O  Array of MACH #'s
      REAL          AREPFL(101,*)      !  O   Array RE Per Foot L
      REAL          QRAT(101,*)        !  O   Q RATio
      REAL          CPMIN              !  O   CP MINimum
C
C SUBROUTINES
C     NAME          DESCRIPTION
C.....................................................................
C     PMEYER
C     SHKREL
C
C ENVIRONMENT
C     Machine:                IRIS 4D
C     Operating System:       UNIX
C     Language:               FORTRAN 77
C
C AUTHOR
C     David pessin
C     Cal Poly, SLO
C
C CHANGE HISTORY
C     DATE          DESCRIPTION
C.....................................................................
C     Sept 92  dnp  Original release - MOD 0.
C
C-*******1*********2*********3*********4*********5*********6*********7**
C
C COMMON PARAMETER VALUES
C     TYPE          VARIABLE            DESCRIPTION
```

```
C.....................................................................
C     none
C
C LOCAL DECLARATIONS
C     TYPE          VARIABLE        VAL  DESCRIPTION
C.....................................................................
C
      REAL          TURNANG           !  flow TURN ANGle
      REAL          CP                !  Coefficient of Pressure
      REAL          M1                !  local upstream Mach number
      REAL          M2                !  local Mach number
      REAL          V2                !  local Velocity
      REAL          P1                !  local upstream Pressure
      REAL          P2                !  local Pressure
      REAL          T1                !  local upstream Temperature
      REAL          T2                !  local Temperature
      REAL          RHO2              !  downstream density
      REAL          PRAT              !  Pressure RATio
      REAL          TRAT              !  Temperature RATio
      REAL          RHORAT            !  density RATio
      REAL          X(3),Z(3)         !  cartesian coordinates
      LOGICAL       SEPARATED         !  flow is SEPARATED if true
      INTEGER       IZ                !  I counter
      INTEGER       IPHI              !  IPHI counter
      INTEGER       I,J,K             !  counters
C
C
C
C=====================================================================


      OPEN(77, FILE = 'FAIRANAL.OUT')
      WRITE(77,*) "IZ,IPHI, TURNANG, M1, M2, PRAT, CP"

      CPMIN = -1 / (MINF*MINF)
```

```
      DO 651 IPHI = IPHIE, NPHI

         SEPARATED = .FALSE.
         M1 = AAMACH(AIZF(IPHI),IPHI)
         P1 = APF(IPHI)
         T1 = ATF(IPHI)

         DO 751 IZ = AIZF(IPHI),NI(IPHI)


            IF ( IZ .NE. NI(IPHI) ) THEN
               DO 26 I = 1,3
                  K = IZ+I-2
                  X(I) = RL(K,IPHI) * SIN( OMEGL(K,IPHI) )
                  Z(I) = RL(K,IPHI) * COS( OMEGL(K,IPHI) )
26             ENDDO
               TURNANG = ATAN((X(3)-X(2))/(Z(3)-Z(2))) -
     1                   ATAN((X(2)-X(1))/(Z(2)-Z(1)))
            ENDIF

            IF ( IZ .EQ. 1 ) THEN
               TURNANG = ATAN((X(3)-X(2))/(Z(3)-Z(2)))
               M1 = MINF
               P1 = PINF
               T1 = TINF
            ENDIF

            IF ( TURNANG .LT. -.35 .OR. SEPARATED ) THEN

               IF ( MINF .GT. 8.0 ) THEN  ! If expnasion angle <
                  CP = 0.0                ! 15 deg, then cp =
               ELSE                       ! some default value.
                  CP = CPMIN              ! flow is separated
               ENDIF
               SEPARATED = .TRUE.
               M2 = 0
```

```
            P2 = PINF
            T2 = TINF

         ELSE                          ! Tan Prandtl-Meyer Ramp

            CALL PMEYER (TURNANG, GAMA, M1, M2, PRAT, TRAT)
C            WRITE(*,*) IZ, IPHI, CP
            P2 = P1*PRAT
            T2 = T1*TRAT
            CP = (P2/PINF - 1.0) / (0.5*GAMA*MINF*MINF)

            IF ( CP .LT. CPMIN ) THEN
               CP = CPMIN
               SEPARATED = .TRUE.
               M2 = 0
               P2 = PINF
               T2 = TINF
            ENDIF

         ENDIF

         WRITE(61,*) IZ,IPHI,CP,TURNANG,PRAT
         WRITE(76,*) ARHORT(IZ,IPHI)

         ACP(IZ,IPHI) = CP
         RHORAT = (P2/PINF)**(1./GAMA)
         ARHORT(IZ,IPHI) = RHORAT
         RHO2 = RHOINF*RHORAT
         AAMACH(IZ,IPHI) = M2
         VRAT = M2/MINF
         V2 = M2*49.1*SQRT(T2)
         AREPFL(IZ,IPHI) = RHO2*V2*(T2+200)/(2.27E-8*T2**1.5)
         QRAT(IZ,IPHI) = (P2/PINF)*(VRAT)**2

         IF ( AREPFL(IZ,IPHI) .LE. 10 ) AREPFL(IZ,IPHI) = 10
```

```
            WRITE(77,770) IZ,IPHI,TURNANG*57.3,CP,M2

            M1 = M2
            P1 = P2
            T1 = T2

  751     ENDDO
  651 ENDDO

  770       FORMAT (2(1X,I3),4(1X,F8.4))
  771       FORMAT (2(1X,I3))



C=======================================================================

      CLOSE (77)
      RETURN
      END

C********1*********2*********3*********4*********5*********6*********7**
```

Elevator Generation Routines for HAVOC

Section of Subroutine AEROANAL

Subroutine AEROANAL is the Aerodynamic Analysis portion of HAVOC. The following short section checks each individual panel to see if it is part of the elevator. If the panel is, then subroutine ELEVATOR is called.

```
C Recompute normals for panels that will be part of Elevators
C Check to see if panel falls within boudaries of elevator
C
            IF ( XA(I) .GT. XA(1)+BLEN*(1 - ELEVLEN) .AND.
     1          ABS(YA(I,J)) .GT. BWID*ELEVIN          .AND.
     2          ABS(YA(I,J)) .LT. BWID*ELEVOUT )CALL ELEVATOR(ELEVAOD2,N)
```

Subroutine ELEVATOR

Subroutine ELEVATOR, called by AEROANAL, changes the normal of the panel by a user specified angle before the pressure coefficient for that panel is calculated.

```
C********1*********2*********3*********4*********5*********6*********7**
      SUBROUTINE ELEVATOR(AOD,N)
C
C ACRONYM
C     ELEVATOR
C     ********
C
C PURPOSE
C
C Make elevators on the rear of the waverider.
C
C
C
C ARGUMENTS
C     TYPE          VARIABLE       I/O  DESCRIPTION
C.....................................................................
C
      REAL          AOD        !  I   Angle Of Deflection, positive up
      REAL          N(3)       ! I/O  Normal Vector
C
C SUBROUTINES
C     NAME          DESCRIPTION
C.....................................................................
C    none.
C
C ENVIRONMENT
C     Machine:               IRIS 4D
C     Operating System:      UNIX
C     Language:              FORTRAN 77
```

```
C
C AUTHOR
C     David pessin
C     Cal Poly, SLO
C
C CHANGE HISTORY
C     DATE          DESCRIPTION
C.....................................................................
C     Nov 92  dnp  Original release - MOD 0.
C
C-*******1*********2*********3*********4*********5*********6*********7**
C
C COMMON PARAMETER VALUES
C     TYPE          VARIABLE              DESCRIPTION
C.....................................................................
C     none
C
C LOCAL DECLARATIONS
C     TYPE          VARIABLE        VAL  DESCRIPTION
C.....................................................................
C

      REAL          NTMP          !  Normal TeMPorary in Z' direction
      REAL          THETA         !  Angle between Z and Z'
      REAL          DEGRAD        !  conversion from degrees to radians
      PARAMETER     (DEGRAD = .017453293)
      REAL          PI
      PARAMETER     (PI = 3.14159265)
C
C
C
C=====================================================================

C
C If bottom surface, calculate different from bottom surface
C
```

```
          IF ( N(3) .LT. 0 ) THEN
             NEG = -1
          ELSE
             NEG = 1
          ENDIF

C
C Transform coordinates so that normal is in X-Z' plane only( N(2)=0 )
C
          NTMP = NEG*SQRT( N(2)*N(2) + N(3) * N(3) )
          THETA = ASIN( N(2)/NTMP )

C
C Perform deflection in the X-Z' Plane
C
          N(1) = SIN( ASIN(N(1))+NEG*AOD*DEGRAD )
          NTMP = NEG*COS( ACOS(NEG*NTMP)+AOD*DEGRAD )

C
C Transform back to X-Y-Z Coordinates
C
          N(2) = NTMP*SIN(THETA)
          N(3) = NTMP*COS(THETA)

C=======================================================================

        RETURN
        END

C********1*********2*********3*********4*********5*********6*********7**
```

CAL POLY
San Luis Obispo

MASTER'S THESIS/PROJECT REQUIREMENT

Student Name **David Neil Pessin** Date Submitted **4-6-93**

Address **255 Marcello Avenue** Phone **498-4634**

Thousand Oaks, CA 91320 School **Engineering**

Degree Objective **Master of Science in Aeronautical Engineering**

Thesis/Project Report Title **Aerodynamic Analysis of Hypersonic Waverider Aircraft**

==========

I. Academic Programs Office

This copy of a thesis/project report has been reviewed and meets the format requirements established by the University. A binding instruction sheet and a fee receipt for binding and microfiche are attached.

Special Instructions:

Thesis Editor — Date 4-6-93

==========

II. Library Administration Office

The University Library has seen the receipt for binding and microfiching and accepts this thesis/project report as meeting library requirements.

Library Director — Date 4-6-93

==========

White: Academic Programs Office
Pink: Records Office
Blue: Graduate Coordinator
Yellow: Student
Green: Library

AP--86